# $^{235}$U Fission Product Decay Heat from 1 to $10^5$ Seconds





EPRI

Keywords:
$^{235}$U Decay Heat
Gamma and Beta Ray
After Heat

EPRI NP-180
Project 392-1
Final Report
February 1976



Prepared by
IRT Corporation
San Diego, California

# $^{235}U$ FISSION PRODUCT DECAY HEAT FROM 1 TO $10^5$ SECONDS

NP-180
(Research Project 392-1)

Final Report

February 1976

Prepared by

IRT Corporation
P.O. Box 80817
7650 Convoy Court
San Diego, California 92138

Principal Investigators
S. J. Friesenhahn
N. A. Lurie
V. C. Rogers
N. Vagelatos

Prepared for

Electric Power Research Institute
3412 Hillview Avenue
Palo Alto, California 94304

Project Manager
Frank Rahn

ABSTRACT

The absorbable components of the fission-product decay heat from thermal-neutron fission of $^{235}U$ have been measured in the 1 to $10^5$ second time range for a one-day (86,400 second) irradiation time. The systematic uncertainty of the measurement is 2.4%, with statistical uncertainties of 2% at 1 second, increasing to 4% at $10^5$ seconds. The measurements were made using a "nuclear calorimeter" which is based on a large (4000 liter) liquid scintillator. The uranium irradiations were made in a water-moderated $^{252}Cf$ source with a rapid pneumatic system to transfer the irradiated sample to the scintillator.

CONTENTS

ILLUSTRATIONS

TABLES

## Section 1

## INTRODUCTION

The present uncertainty in the $^{235}U$ thermal-neutron, fission-product decay heat which must be removed after reactor shutdown is of major economic importance. This results from the fact that plant design requires a conservative allowance for the maximum possible heat load. A recent review of existing fission-product decay heat measurements by Perry et al. (1) has pointed out these uncertainties.

The present work is directed toward a measurement of decay heat which will be of use not only in direct prediction of shutdown heat load, but also as a test case for decay heat summation calculations, such as those currently underway by Spinrad (2).

The problem of fission-product decay heat measurement has been traditionally approached in one of three ways.

1. Thermal Calorimeter. The irradiated sample is brought to the center of a mass of material sufficient to absorb most of the beta and gamma radiation, and the temperature rise of the mass is recorded. Examples of this technique are the measurements of Gunst et al. (3) and Lott et al. (4), as well as measurements currently in progress at the University of California at Berkeley (L. Grossman et al.) and Los Alamos Scientific Laboratory (J. L. Yarnell et al.).

2. Nuclear Spectroscopy. The irradiated sample is brought to a point sufficiently distant from a spectrometer such that single beta or gamma events may be recorded. The decay heat is calculated from the response function unfolded data using the measured spectrometer efficiency. Examples of such measurements are those of Bunney and Sam (5) and Tsoulfanidis et al. (6), as well as work currently in progress at Oak Ridge National Laboratory (J. K. Dickens et al.).

3. Summation Calculations. Radiochemical separation of the irradiated sample is performed to arrive at a detailed understanding of fission product yields and decay chains, from which the decay heat is calculated.

The techniques reported here are somewhat different from those just described. The present experiment is a "nuclear calorimeter" technique in which the advantages of techniques (1) and (2) above are combined to yield a precise direct measure of the decay heat. Figure 1 illustrates these advantages.

Briefly, the method is as follows. Samples of $^{235}U$ were irradiated in a thermal-neutron flux produced by a water-moderated $^{252}Cf$ source for a specified time. Following irradiation, the samples were transferred by a pneumatic system to a very large, total absorption scintillation detector which absorbs virtually all of the beta and gamma radiations, and produces a light signal directly proportional to the energy absorbed. Corrections for the small energy losses in the system were made using a combination of measured and calculated correction factors. The number of fissions was determined using a specially designed ion chamber.

In the following sections more detailed information is given on each of the major components of the experimental apparatus and the procedures used in the present program. In addition, there is a description of the calculations performed in support of the experiment. Finally, the results for the measured $^{235}U$ fission-product decay heat are presented and compared to calculation and the ANS standard. A discussion of the estimated uncertainties and recommendations for further improvement are also given.

MERITS OF THREE POTENTIAL MEASUREMENT TECHNIQUES

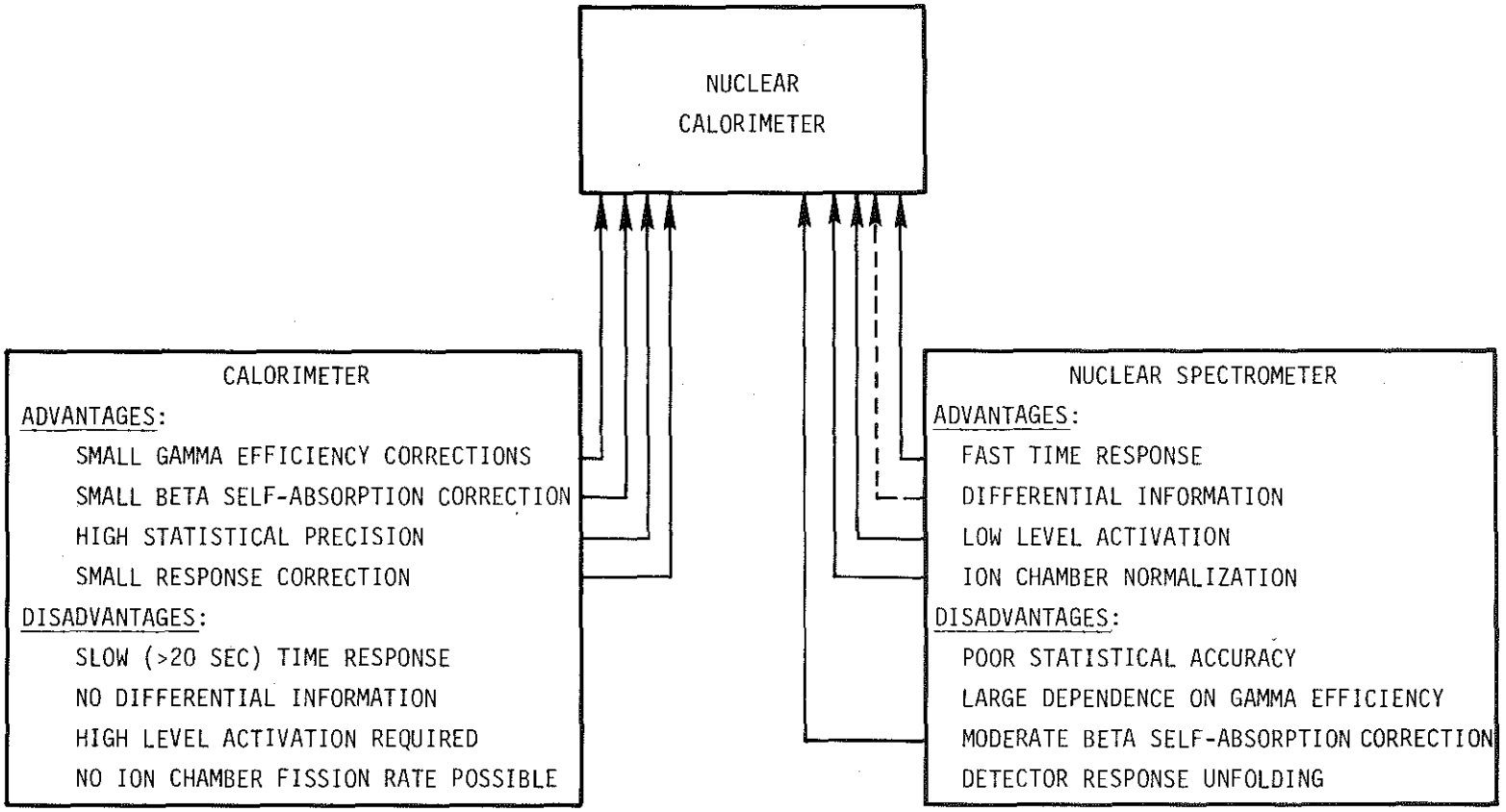


Figure 1. Advantages and disadvantages of nuclear calorimeter versus other fission product decay measurement techniques.

## Section 2

## EXPERIMENTAL APPARATUS AND PROCEDURES

### 2.1 NUCLEAR CALORIMETER

The nuclear calorimeter is a very large (4000 liter) liquid scintillator which has been described previously in the literature (7). The scintillator was constructed for the purpose of neutron-capture cross-section measurements. Such measurements require not only a high efficiency for the detection of neutron-capture gamma-ray cascades, but also a uniform response and reasonably good gamma-ray energy resolution. To satisfy the latter two requirements, the scintillator was constructed in modular form (Figure 2).

Each module is a thin-walled plastic cylinder viewed at each end by photomultiplier tubes. The cylinders are filled with a decahydronaphalene-based liquid scintillator. The light collection efficiency is relatively high and uniform. The light collection properties have been reported previously in the literature (8).

Forty-four 9-inch-diameter cylinders (logs) are arranged in a close packed array around a central 24-inch-diameter central cylinder (center section). The cylinders all have a 60-inch active length and a 9-inch-long light pipe on each end. Further details of the construction and performance of this scintillator are given in References 7 and 8.

For the purposes of the present work, a 6-inch-diameter, 16-inch-long NE110 plastic scintillator was located at the center of the central liquid scintillator. This plastic scintillator was fabricated with a reentrant hole which forms the terminus of the pneumatic transfer (rabbit) system. This rabbit system is capable of transferring an irradiated sample into the center of the plastic scintillator within one second.

The plastic scintillator does not employ a light reflector in the reentrant hole, but the outer surface of this scintillator, as well as all the liquid

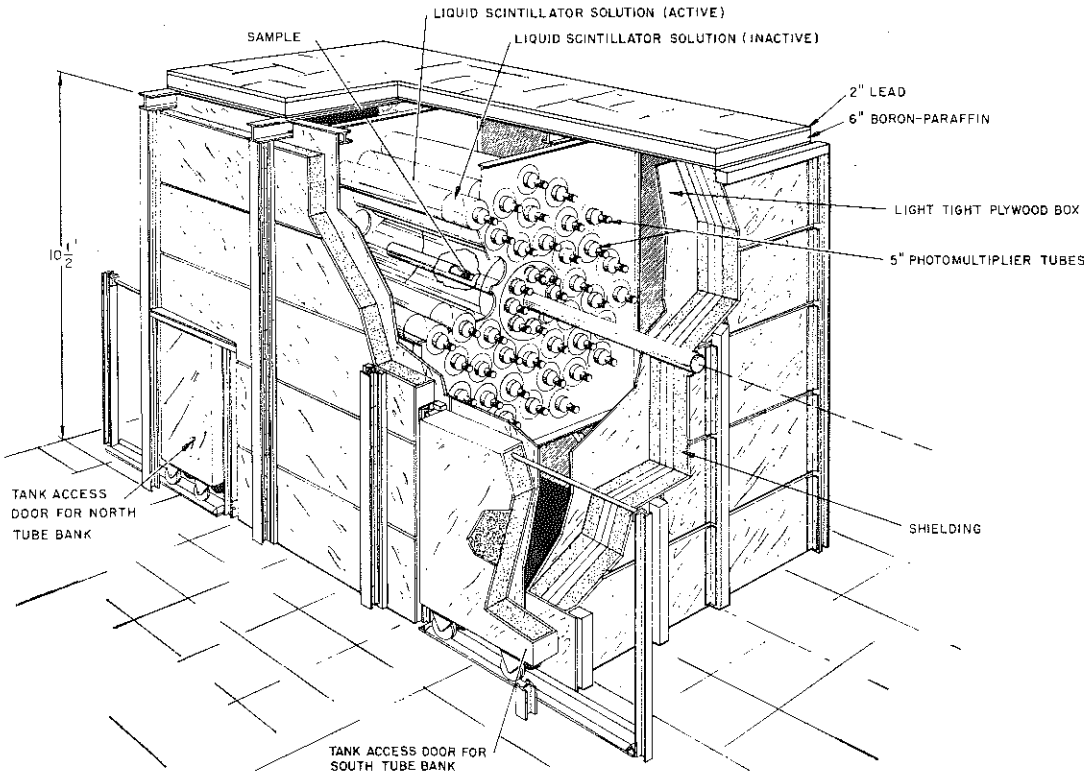


Figure 2. Illustration of scintillator construction.

scintillators, are covered with aluminum foil reflectors which not only improve uniformity of response, but also allow each component of the system to be operated independently. The advantages of such operations will be apparent shortly.

## 2.2 IRRADIATOR

One of the advantages of using a high efficiency nuclear detector is that usable fission-product decay signals can be obtained at only moderate neutron flux levels. For this reason, a 10-milligram $^{252}Cf$ source which produces a flux of $\approx 1 \times 10^8$ thermal neutrons/cm$^2$/sec has been used exclusively for these measurements. The neutron emission is of course very constant, decaying with a 2.6-year half life.

The water which provides the majority of the moderation of the spontaneous fission spectrum from the $^{252}Cf$ is continuously filtered through particulate and activated charcoal filters to ensure a constant purity. The source is positioned in a lead block which is immediately outside a 4-inch-diameter dry well. This dry well contains either the irradiation end of the rabbit system or an ion chamber, which is described in Section 2.6. The rabbit tube is surrounded by several polyethylene rings which provide additional neutron moderation and serve to hold the irradiation tube in position. The 0.01-inch cadmium ratio at the irradiation position is approximately 25, and hence the perturbation of the fission yield due to epithermal neutrons is negligible.

The neutron flux in the irradiation tube was monitored with a $^{235}U$ coated cylindrical ion chamber which drove an electrometer readout. The neutron flux was found to be steady, and decayed with the expected half life. The method employed here for calibration did not require that the absolute value of the flux be accurately known, but only that it remains constant.

The samples of $^{235}U$ used for the present study were in the form of a uranium-aluminum alloy containing 22.8 wt % $^{235}U$. The isotopic analysis of the uranium is given in Table 2-1. Details of the mounting and dimensions are discussed in Section 2.6.

Table 2-1

ISOTOPIC ANALYSIS OF URANIUM IN ALLOY FOILS

| ISOTOPE | ATOMIC PERCENT |
|---|---|
| 234 | 1.113 |
| 235 | 93.26 |
| 236 | 0.259 |
| 238 | 5.37 |

## 2.3 RABBIT SYSTEM

The pneumatic transfer system is responsible for the rapid transfer of an irradiated sample into the scintillator for the initial measurement. After completion of the initial measurement, the sample is stored in one of five locations in a motor driven carriage (receiver). When the time for the next measurement on this sample arrives, the receiver is first positioned to the storage location for a $^{60}Co$ standard source. This is a National Bureau of Standards calibrated source which has been covered with 0.03 inch of Mylar to absorb the 300-keV beta radiation. This standard source is transported into the scintillator, and the net signal is taken to be proportional to the energy emission rate of the 1.173 + 1.332 MeV gamma rays.

Immediately after the scintillator calibration, the receiver positions the appropriate $^{235}U$ sample for transfer into the scintillator for the fission-product decay measurement. The data accumulation techniques are described in detail in Section 2.4.

The air supply to operate the system is supplied by a 1¼-inch-diameter line from the 90 psi building air supply. The pressure is reduced to 10 psi by a pressure switch and solenoid air valve, which is capable of keeping a

10-gallon reserve tank within 1 psi of the desired value, even when the transfer system is operating at its maximum rate.

Air is introduced into the 1-1/8-inch polyethylene transfer lines by a fast acting, bidirectional solenoid valve. The valve is actuated by the unregulated 90 psi air. Smooth and reliable transfers are accomplished by precise (±1 millisecond) computer control of the opening and closing times of the solenoid valve.

Transfers from the irradiator to the scintillator are accomplished in approximately 0.8 seconds, with acceleration air pressure applied for 0.30 seconds. When the rabbit reaches a rubber cushion in the scintillator a switch is actuated which operates a solenoid valve which, in turn, vents the downstream air from the rabbit system. This downstream air provides some deceleration in the 0.30 to 0.80 second interval, and it must be vented to prevent rebound of the rabbit. The scintillator switch also signals the computer that a successful transfer has been accomplished. Similar switches are located at the irradiation end, as well as at each of the six receiver storage locations.

The receiver location is sensed by three photocells which view light bulbs through a series of 0.03-inch-diameter holes in a bar attached to the receiver carriage. The holes are coded in a binary pattern which allows the computer to sense the location of the carriage, and to stop the carriage at the correct moment. Positioning accuracy is $\approx \pm 1/32$ inch.

## 2.4 DATA ACQUISITION

The complexity and time span required for these measurements preclude the manual operation of the experiment. Instead, all operations are controlled by a Hewlett-Packard 2116B computer. The peripheral equipment includes a fixed head disk, line printer, teletype, analog plotter, card reader, digital plotter, storage display scope, and a data multiplexer which allows the addressing of several additional pieces of equipment, including an 8192-channel analog-to-digital converter (ADC).

The data acquisition program is written in five segments which are called from the disk by the operating system as needed. This results in a considerable saving in core memory space, and hence a marked increase in the system

capability. The logic flow diagram for data acquisition is illustrated in Figure 3. The majority of the startup input information is read from the card reader. Included in this information is the date and time at which the irradiation of each sample terminated. This information is used to keep track of the cooling time of each sample. A 100-point measurement time mesh is also input which is used to determine when a given sample should be measured.

After the startup information is input, the operator can request that a new sample be brought from the irradiator. This transfer can either be a fast (<1 second) transfer from the rabbit irradiator or a slow transfer by hand (∿45 seconds) of an ion chamber foil.

In either case, the program first adjusts a programmed power supply current which is summed in opposition to the scintillator current (Figure 4). The difference is adjusted to fall within channels 500 to 1000 of the ADC to ensure that the system is in the linear range of the instrument. This bucking current is then turned off, along with the signal from the outer region of the liquid scintillator. Background current measurements are then made for the plastic scintillator, the surrounding central liquid scintillator, and the logs. The standard $^{60}Co$ source rabbit is inserted, and the net signal for each of these three units is measured. If the ratio of the net currents from the plastic versus the central scintillator differs by more than 1% from the input ratio, a gain adjustment is made on the plastic scintillator until agreement is achieved. In this way we avoid the majority of the error which might result if the plastic scintillator response changes. This response represents all of the beta-ray signal, but only a small part of the gamma-ray signal, whereas the liquid scintillator responds primarily to the gamma-ray component. A 1% error in the balance results in a 0.3% error in the measurement.

After the plastic scintillator balancing is complete, the program restores all signals and performs a calibration using the $^{60}Co$ rabbit. The background is read before each insertion and after each removal of the rabbit, and the foreground/background measurement cycle is repeated ten times to allow an estimate of the standard deviation of the measurement to be made. The average of the ten net current readings is taken to be proportional to the $^{60}Co$ gamma energy deposition rate after correcting for the 5.261-year half life of this isotope.

COMPUTER CONTROLLED DATA ACQUISITION LOGIC DIAGRAM

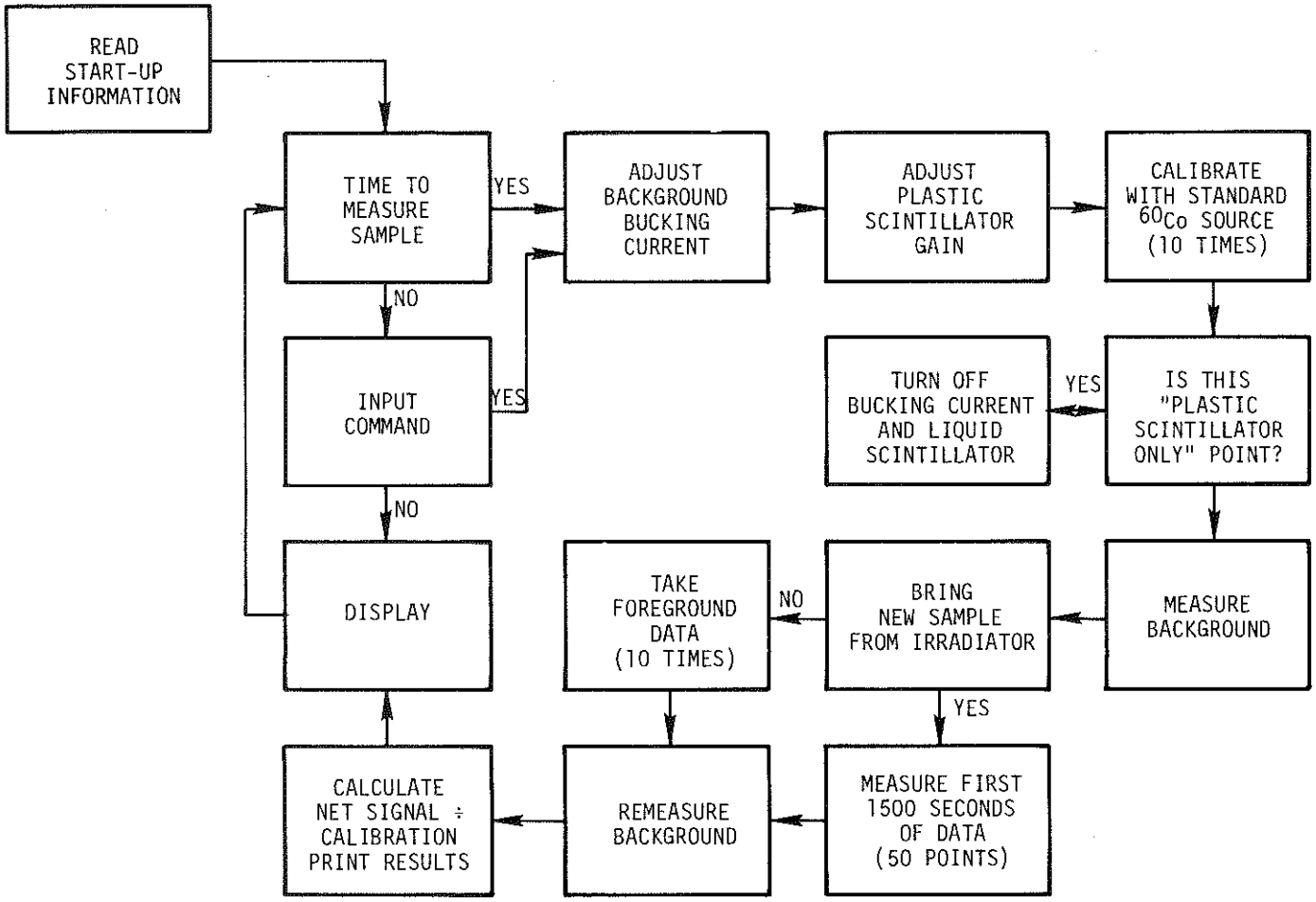


Figure 3. Logic diagram of data acquisition code.

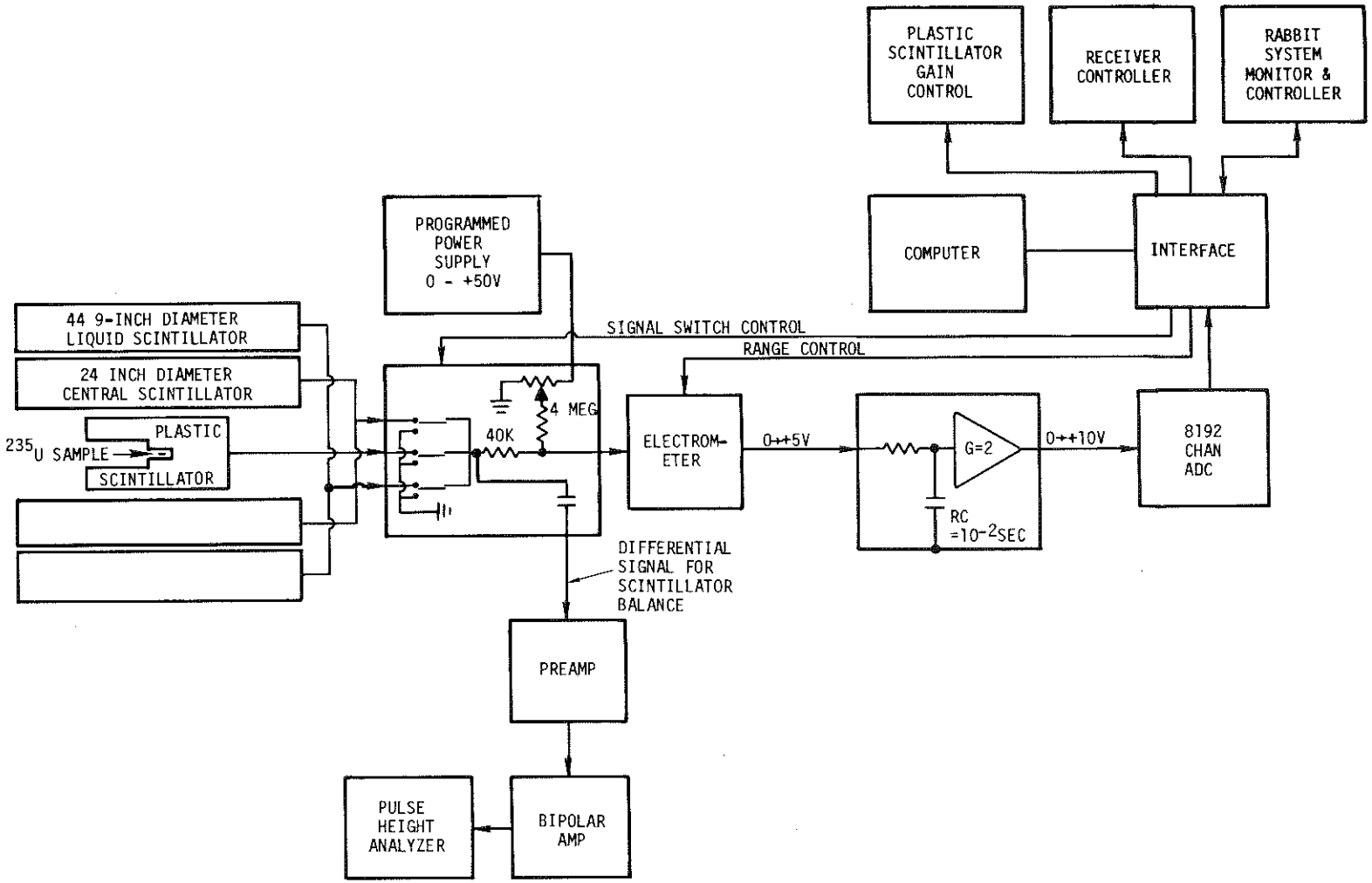


Figure 4. Signal processing diagram.

If a new sample is to be brought from the irradiator the program requests that the operator make the appropriate hose connections, after which the background is read and the irradiated sample brought into the scintillator. Since the fission-product decay is relatively rapid at early times, it is not feasible to cycle the rabbit rapidly enough. For this reason, the first 1500 seconds of data are taken in 50 equal logarithmic time increments. Since the scintillator gain drift is typically 4%/12 hours, the gain shift during this time is less than 0.2%. At the end of this period the rabbit is stored in the next available receiver location, and the background is remeasured. Some or all of the 50 points may be taken with only the plastic scintillator on for the purpose of calibrating the number of fissions, as explained in Section 2.6. In any event, the $^{60}Co$ calibration is performed with the entire scintillator on. The random component of the standard deviation of these points is estimated from the variance of the calibration, the change in the background, and the scatter of the measured points. This scatter is calculated relative to interpolations between neighboring points.

If a previously irradiated sample is being brought from the receiver, the measurement process is exactly the same as that for a $^{60}Co$ calibration determination. Again, some points may be taken with only the plastic scintillator on. In any event, the standard deviation is calculated for each point using the variance of the calibration and the variance of the signal.

## 2.5 SIGNAL PROCESSING

The anodes of the 109 photomultipliers used in the scintillator are divided into "north" and "south" banks according to the geographic orientation of the cylinder on which they are mounted. The five photomultiplier tubes on the plastic scintillator (four 2-inch tubes on the north end surrounding the rabbit tube, and a 5-inch tube on the south) are connected in parallel via coaxial cable and are brought to a computer controlled relay at the signal junction box (Figure 4). The 16 tubes on the central liquid scintillator are paralleled to form the "center section" signal, and the 88 tubes on the logs form the third (log) signal source. These two combined signal sources are brought through two additional relays at the junction box. The outputs of these three relays drive the input of a Kiethly 410C electrometer through a 40,000-ohm resistor. The resistor provides some integration of the signal to avoid saturation of the electrometer amplifier by the large cosmic-ray signals from the scintillator.

The 0 to +5 V "recorder signal" output from the electrometer is routed to the computer room located approximately 100 ft away. Here the signal is integrated with a 10-millisecond time constant at the input of an operational amplifier. The 0 to +10 V output of this amplifier is the input to the 8192-channel ADC. Even after this additional integration the signal is characterized by substantial fluctuations about the mean valve. These fluctuations are due to statistical fluctuations in the scintillator signal as well as noise pickup on the transmission lines. For this reason, the computer samples the signal every 2.5 milliseconds and averages the result to form the value used by the data acquisition program. Since the sample period is appreciably shorter than the integration time, the resultant average is statistically efficient in that longer integration will not provide more information.

The average background signal from the scintillator is approximately 3 μA. In some cases the signal to be measured is appreciably smaller than this, and hence the programmed power supply output is summed with the scintillator signal at the input of the electrometer. This positive current is adjusted by the computer to be slightly less than the background, so that the electrometer can be operated with a sensitivity which makes best use of the dynamic range of the ADC.

The plastic center section balancing operation is best performed with a 3-μA sensitivity on the electrometer. For this reason, the electrometer was modified to allow the computer to force it into the 3-μA range, regardless of the manual setting of the sensitivity.

Since the signal gains of the photomultipliers are not in general the same for each tube, the gains are adjusted prior to a measurement by a variable resistor in series with each tube. The radiation source for the log-balancing operation is the 4.4-MeV gamma ray from a PuBe source located at the center of the scintillator. An individual photomultiplier may be turned on by a switch matrix, which allows its gain to be measured utilizing the differential recording system indicated in Figure 4. The Compton edges from the individual tubes are matched with a precision of ±5%. This precision is comparable to the longitudinal nonuniformity of the cylinders (8).

The PuBe source activity is too high for use with the central scintillator, and hence a $^{24}Na$ source is used for balancing its 16 tubes. The central

scintillator is then itself balanced against the sum of all 44 logs using the 1.57-MeV $^{142}Pr$ line, taking advantage of the fact that this unit is driven by a separate power supply.

Cobalt-60 is most suitable for adjusting the five tubes on the plastic scintillator and the subsequent balancing of this unit against the central scintillator. This balancing is achieved with a 1% precision by using calculated responses for these two units. (Calculations are described in Section 3.) A special differential data acquisition code (RFCS) compares the measurement to a resolution-broadened, calculated curve. The resolution width and energy scale are adjusted to obtain a satisfactory match between calculation and experiment.

After the plastic and liquid scintillators have been so balanced, the ratio of the net signal from the two units produced by the standard $^{60}Co$ source is measured. This ratio is then used by the main data acquisition code to maintain this balance during data acquisition.

The balancing just described was performed with gamma rays, and it is necessary to determine the relative response of the plastic scintillator to beta particles. This response may be slightly different due to surface damage produced by the polishing of the plastic scintillator, and to differences in light collection from events depositing their energy very close to the reentrant hole in the plastic.

The electron spectrum from $^{137}Cs$ is a convenient source for such study, since it consists of a single internal conversion line superimposed on two beta spectra. A NBS standard source was used, which is a very thin ($\approx$0.001 inch) source sandwiched between 0.002-inch Mylar layers. This material, along with an additional 0.002 inch of Mylar, was used in a transport calculation (see Section 3) to determine the emergent electron spectrum. A good match between calculation and experiment was achieved for the internal conversion line, but there is a residual disagreement with the shape of the beta spectrum. This discrepancy has not been fully investigated at this writing (Figure 5). In view of the small contribution of very low energy beta particles to the beta dose, the assumption of a constant beta energy scale below the 600-keV internal conversion line is not deemed a significant source of error.

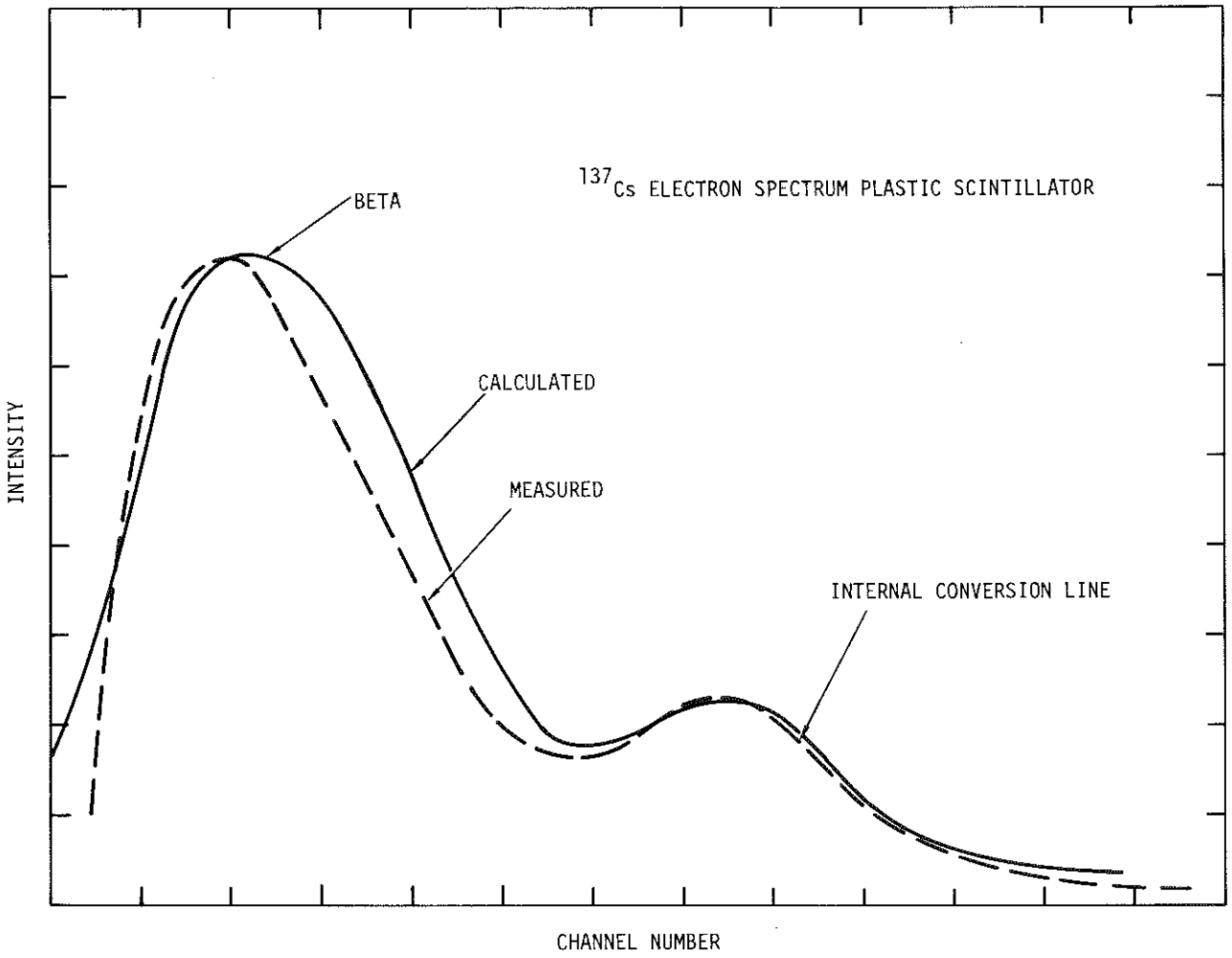


Figure 5. Calculated versus measured $^{137}C_s$ electron spectrum in plastic scintillator.

## 2.6 ION CHAMBER

The system thus far described is capable of forming a signal proportional to the fission-product decay power. This energy emission rate P must be interpreted in terms of the fission power $P_o$ which existed during irradiation. A common method of accomplishing this is the counting of individual gamma-ray lines from fission products with known yields and decay schemes. This method suffers from a host of experimental uncertainties, and a direct determination of the fission rate is potentially more accurate.

Clearly, the fission products cannot be detected during the irradiation, since they must be confined in the sample assembly. For this reason, a direct determination of the fission rate by pulse counting in an ion chamber involves either a measurement before or after completion of the fission-product decay heat measurement, or a measurement in a second sample and a cross normalization.

An accurate fission rate determination in an ion chamber requires that very high fission bias efficiency be achieved, since the shape of the pulse-height distribution at low amplitude is not known *a priori*. This shape is sensitive to small imperfections in the surface of the fission foil which are not easily calculated.

High bias efficiency in the present work has been achieved by using thin deposits (137 $\mu g/cm^2$) of very high purity $^{235}U$ (99.89%) on very thin nickel substrates (0.00002 inch, $\approx$500 $\mu g/cm^2$); Table 2-2 gives the isotopic analysis of the uranium deposited. These foils are necessarily very fragile, and this prevents their use after the rough handling in the rabbit system. The measurement of the fission rate before introduction into the rabbit system is potentially the most accurate, provided that the slight activation of the foil due to retained fission products is allowed to die away before the final irradiation starts. This technique was not normally used, since it destroys one foil permeasurement, and only a limited number of foils were available.

For these reasons, the cross normalization technique was used in measurements reported here. Some of the evaporated foils were encapsulated between 0.002-inch Mylar covers (Figure 6). The Mylar covers were coated with a thin coat of epoxy resin and immediately applied to both sides of the foil. An additional pair of covers were then cemented on either side with Pliobond cement

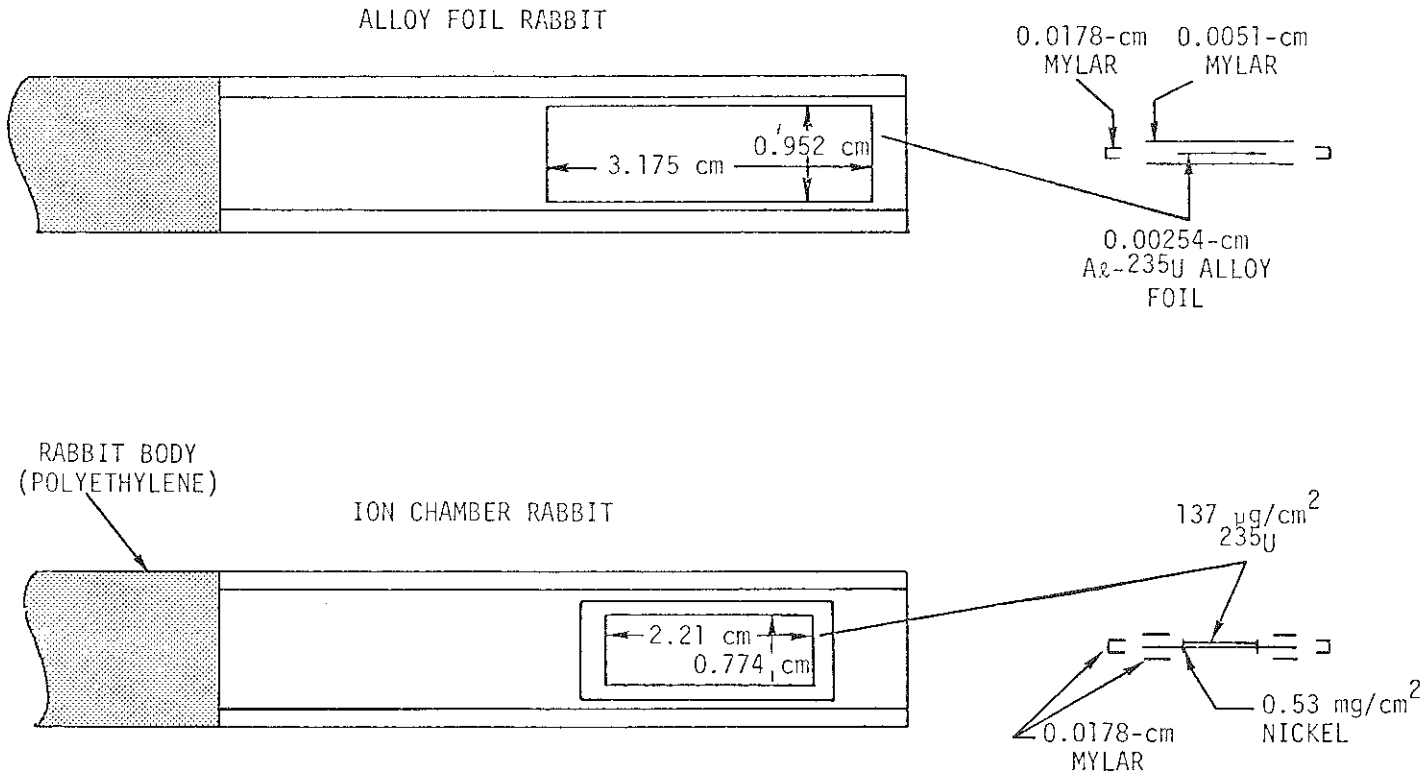


Figure 6. Rabbit and sample assembly.

to improve the mechanical integrity. The resultant assembly is impervious to leakage of volatile fission products. As an indirect check on this assumption, a foil encapsulated in the above fashion was counted in the ion chamber. The resultant count rate was $\approx$0.5% of the fission rate, and consisted of small pulses, probably due to straggling of the low-yield light fragments through the Mylar.

Table 2-2

ISOTOPIC ANALYSIS OF URANIUM IN ION CHAMBER FOILS

| ISOTOPE | ATOMIC PERCENT |
|---|---|
| 233 | <0.0005 |
| 234 | 0.034 |
| 235 | 99.89 |
| 236 | 0.025 |
| 238 | 0.052 |

The ion chamber is our own design; construction details are illustrated in Figure 7. The fission foil, mounted on a standard rabbit assembly, is lowered in through a hole in the top of the chamber by a metal rod. The foil makes contact with a spring which is connected to a -1500 V polarizing power supply. The fission particles escape from both sides of the foil, one of the particles having passed through the nickel substrate. The free electrons resulting from the ionization drift through the argon – 10% $CO_2$ counting gas mixture – and pass through the Frish grids located on either side. The grids are wound with No. 37 aluminum wire spaced 0.1 inch apart, and hence collect few of the electrons. The grids operate at ground potential. After passing the grids, the electrons are collected on two collector plates tied in parallel to the input of an ORTEC 125 preamplifier. The collectors are polarized at +400 V through the preamp bias supply. The preamp output is fed to an ELSCINT bipolar amplifier with a 1.6-μsec shaping time constant.

The interior of the chamber is lined with 0.03-inch lead foil, and the grid frames are fabricated from Plexiglas to reduce the background at low pulse height due to beta activation of chamber components. Reduction of background is of importance in obtaining a measure of the shape of the pulse-height distribution to the lowest possible value.

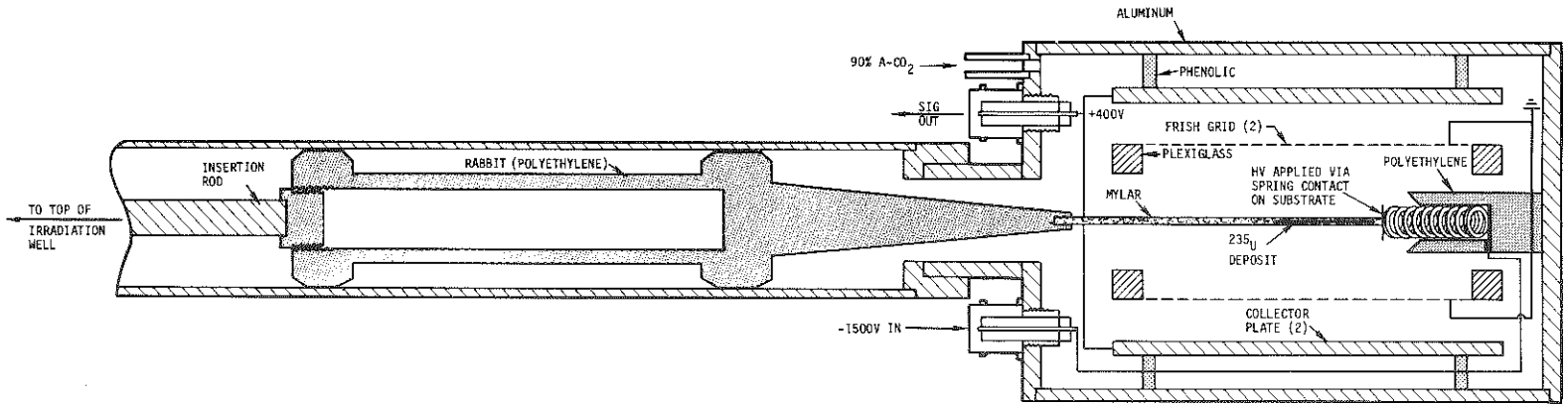


Figure 7. Ion chamber construction

Background components also originate from the buildup of fission products in the chamber, proton recoils from fast neutrons, and charged particle reactions. In an attempt to do the best possible job of background subtraction, an apparatus was fabricated to move the $^{252}Cf$ source $\approx 24$ inches above its normal position under computer control. This apparatus consists simply of a large pneumatic cylinder connected to the rabbit air control system. The cylinder is attached to a stainless steel tube which engages the top of the source by a friction fit. The apparatus moves the source in approximately 2 seconds, and after an additional 4 seconds wait for amplifier gain stabilization, the pulse height is accumulated for 10 seconds of live time. It is thus possible to make fairly accurate subtractions of activation components with reasonably long half lives. The in/out cycle is repeated 25 times.

The fast neutron associated background is subtracted by performing the same operation with the ion chamber covered with cadmium. The measurement is not made until the short-lived activation due to the thermal flux has died away.

The above procedure effectively yields the net ion chamber signal due to prompt reactions due to thermal neutrons. Thus, one further step in the background subtraction is made by replacing the $^{235}U$ foil with a bare foil. These data are then subtracted from the previous data to yield the prompt signal due to thermal-neutron interaction in $^{235}U$, which is almost exclusively fission.

The fission pulse-height distribution is illustrated in Figure 8, with the gain increased a factor of 8 above the linear range of the system. This high gain position is used to examine the shape of the low end of the pulse-height distribution in detail. After the shape of the fission distribution has been established, a discriminator bias is set such that all the low energy backgrounds are biased out. The output of the discriminator drives a specially constructed time gate which allows the desired system deadtime to be established. This time gate has the property of exhibiting a fixed deadtime independent of retriggering time. It thus makes the system an ideally "nonsaturating" system. The time gate is always set to a deadtime greater than the maximum discriminator deadtime (20 μsec).

To correct for the system deadtime, the counting rate is measured with and without a test pulse connected to the input to the preamplifier. It can be shown that the true counting rate in a nonsaturating system is

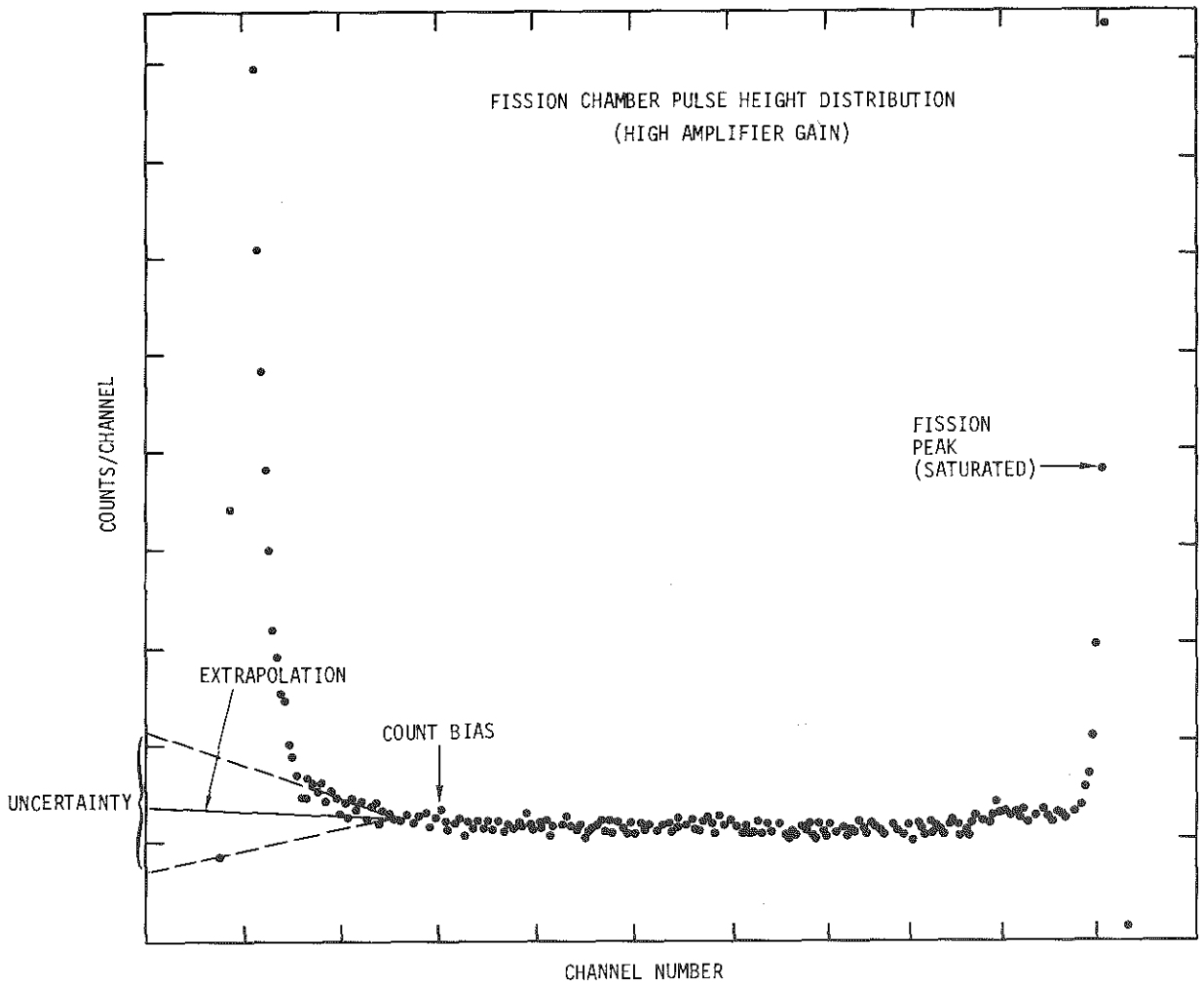


Figure 8. Fission chamber pulse height distributions

$$c = \frac{c'}{\sqrt{\frac{(c+p)' - c'}{p}}} \quad ,$$

where $c'$ is the measured counting rate without the pulser connected, $(c+p)'$ is the measured sum of the random counts and the pulser, and p is the pulser rate. The reliability of the deadtime corrections thus obtained were checked by taking counts with the deadtime set at 20, 40, and 320 microseconds. This results in corrections of 19.7, 40.8, and 442.0%, respectively. The first two values yielded counting rates which agreed within statistics (0.16%), and the latter value 6.3% higher. The assumption of a linear dependence of the error on deadtime correction yields a correction uncertainty of 0.4% for the 20-μsec setting.

Since it is necessary to depend on the reproducibility of the neutron flux at the ion chamber foil position, the chamber is located at the maximum flux position in the dry well. This position can be expected to exhibit a minimum flux gradient, and hence a minimal sensitivity to incidental position changes in the fission foil. The flux gradient was measured by irradiating gold foils in chamber. The maximum gradient determined in this fashion was 1.2%/cm. Since the position reproducibility is better than 0.1 cm, the error due to positioning is assumed to be 0.1%.

Another assumption is that the application of the 0.02-inch Mylar covers does not change the fission rate. In view of the low macroscopic cross section of this material, this assumption is assigned zero error.

Contrary to the purchase order specifications, the supplier of the fission foils (ORNL) did not perform mass determinations on individual foils. Therefore, the relative amount of $^{235}U$ on each foil was measured by counting the 184-keV gamma-ray line on a Ge(Li) spectrometer system to a statistical precision of 0.5%. These relative masses were then used to determine the fission rate in the Mylar-covered fission foils versus the exposed foil.

Since the amount of $^{235}U$ contained in an ion chamber foil is quite small (≈230 μg), the signal produced in the scintillator tends to be small compared to ambient. This would result in undesirably large statistical uncertainties in the decay heat. For this reason, the ion chamber foil data is accumulated

with only the plastic scintillator turned on. Since this unit is relatively small and well shielded by the bulk of the liquid scintillator, the ambient signal is several orders of magnitude smaller than that of the entire system.

All portions of the scintillator are used to accumulate the $^{235}$U-Aℓ alloy foil data since they contain approximately 50 times more $^{235}$U, and hence, produce a net signal with acceptable statistical uncertainty. As explained earlier, the acquisition code can accumulate data from the plastic scintillator only for certain selected cooling times. Eight such points are distributed in the 1 to $10^5$ second cooling time range. These special points provide an overdetermined normalization to the ion chamber foil data. In this way the plastic scintillator is used as a normalization device to obtain the fission rate during the alloy foil irradiation.

## Section 3

## TRANSPORT CALCULATIONS

A small calculational effort was carried out as part of this program. The calculations performed were of the following types.

1. Calculations in support of the experiment design and optimization.
2. Simulation of various checkout and test measurements.
3. Calculation of correction factors to be applied to the data.

Most of the above calculations were performed with the coupled photon electron, Monte Carlo code SANDYL (9). In addition, a new Monte Carlo code to calculate the ion chamber pulse-height spectrum from fission fragments was developed.

### 3.1 DESCRIPTION OF SANDYL

The SANDYL code (9), used for the bulk of the calculations reported here, is a coupled photon electron transport code utilizing the Monte Carlo method. It is capable of following the transport and energy deposition of photons and electrons and their secondaries in complex three-dimensional geometries. We give here only a brief summary of the methods of the code; a more detailed description is given by Colbert (9).

Source particles (either photons or electrons) are generated according to the desired prescription and followed one at a time through the system, with all secondary electrons and photons followed until their energy is degraded below a cutoff value, or until they escape from the system.

Photon histories are treated in the following way. From the properties of the various materials in the system, and using tabulated cross sections, a total interaction probability at the current energy is constructed. This is

randomly sampled to give the next interaction location. An interaction event at this point is chosen from the relative probabilities for photoelectric absorption, coherent scattering, incoherent scattering, and pair production. The angular and energy distributions of any secondaries which may have been produced by the primary event are sampled and stored for later consideration. The process is repeated until either the particle escapes the system or its energy is degraded below a specific cutoff. The secondary photons which result from bremsstrahlung, fluorescence, or annihilation radiation are followed.

For electron transport, the condensed-history method is used (10). With this technique the spatial steps taken by an electron are precomputed and may include the effects of a number of collisions. The corresponding energy loss and scattering angle in the step are found from the tabulated multiple scattering distributions for these quantities. The electron may lose energy through inelastic electron-electron collisions, bremsstrahlung generation, and polarization of the medium. Secondary particles generated in each step result from knock-on, pair production, Auger, Compton-scattered, or photoelectric processes.

## 3.2 ENERGY LOSS IN SAMPLES

Energy lost by the fission product beta rays in escaping from the $^{235}U$ foil itself and in passing through the Mylar covers must be determined so that appropriate correction can be applied. Initial calculations were performed on simple slab configurations to provide guidance in designing the sample, and in selecting thicknesses of sample and covers. The final calculations correspond to the actual sample geometry for the two types of foil: (1) $^{235}U$ deposited on a thin nickel substrate; (2) $^{235}U$-Aℓ alloy (Figure 6).

The calculations were performed in the following way. Since neutron self-shielding effects are small, a spatially uniform distribution of fission-product beta rays was assumed to exist in the uranium; the spectrum was taken to be the 16-group, 0 to 12 second after 8-hour exposure (constant fission rate) measured spectrum of Tsoulfanidis et al. (6).

Transport of the fission-product beta rays and all secondaries was carried out with the SANDYL code. The energy escaping the samples was compared to

the total energy per fission. The percentage of energy lost for the two sample types is summarized in Table 3-1. The calculation was repeated with the longest time (3 hours) after exposure beta-ray spectrum reported by Tsoulfanidis et al. (6).

Table 3-1

BETA-RAY ENERGY LOST IN FISSION SAMPLES

| | | Energy Escaping Sample (MeV/fission) | Percentage Loss |
|---|---|---|---|
| 0-12 second[a] beta spectrum | $^{235}$U on Nickel | 4.678 | 6.07 |
| | $^{235}$U-Aℓ Alloy | 4.685 | 5.93 |
| 10800-11100 sec[b] beta spectrum | $^{235}$U-Aℓ Alloy | 0.240 | 9.94 |

[a]Based on 4.98 MeV/fission and 4.37 electrons/fission (6).

[b]Based on 0.267 MeV/fission and 0.427 electrons/fission (6).

The statistical uncertainty associated with the Monte Carlo calculations alone is less than 0.5%. This is much smaller than uncertainties associated with the measured beta-ray energy spectrum. These results are also limited by the fact that the source beta spectra did not correspond to the actual 24 hr irradiation time used for the present experiments. Spectra for a 24 hr irradiation time are not presently available.

## 3.3 $^{137}$Cs SPECTRA

In support of the scintillator response function studies, it was necessary to calculate the pulse-height spectra in the scintillator for $^{137}$Cs beta rays, as discussed in Section 2. The beta-ray spectrum consists of two groups with endpoint energies of 0.514 and 1.176 MeV, respectively (11). In addition, there is a prominent internal conversion line at 0.624 MeV, with weaker conversion peaks at 0.656 and 0.660 MeV. To provide a source term for the transport calculations, the beta-ray spectra were calculated using Fermi theory with screening corrections and with shape correction factors due to the forbidden nature of the transitions.

The energy deposition spectrum in the plastic scintillator was calculated using a source consisting of the conversion electrons and calculated beta-ray spectra. The effects of the Mylar covers on the source were included in the

calculations. A comparison between the measured pulse-height spectrum and the resolution-broadened calculation is shown in Figure 5. The measured beta-ray spectrum was obtained by subtracting from the total $^{137}Cs$ response in the plastic scintillator the spectrum measured with 3-mm polyethylene covers on the source. A comparison of measured and calculated gamma-ray responses in the plastic scintillator $^{137}Cs$ is shown in Figure 9. The agreement for the gamma-ray spectra is reasonably good, except at low energies. The agreement for the beta-ray case is not entirely satisfactory. It appears as though there is some error in the input source spectrum. At this time the problem has not been resolved.

### 3.4 $^{60}Co$ SPECTRUM

The scintillator energy calibration is performed using a $^{60}Co$ source. $^{60}Co$ decays by double gamma-ray emission, with the cascade consisting of 1.173- and 1.332-MeV gamma rays. Because these two gamma rays are emitted essentially simultaneously, and because the scintillator is a $4\pi$ detector, the energy deposited is largely the sum of these energies. The model of the scintillator includes details of the source holder, plastic scintillator, structural members, and liquid scintillator.

### 3.5 FISSION PRODUCT SPECTRUM

To provide information bearing on the design of the ion chamber and ion-chamber samples, a code was developed which predicts the fission-fragment, pulse-height spectrum in the ion chamber. The procedure used in the code is as follows: A pair of fission fragments is selected at random from the yield distribution. The charge of each fragment and the total kinetic energy of the pair is looked up in a table as a function of mass ratio. The energy table is based on the measurements of Schmitt, Neiler, and Walter (12). The energy is partitioned among the fragments, assuming no momentum is carried by the neutrons. Then the location of the fission event in the foil is chosen at random, as are the directions. The distance to the edge of the foil is calculated, and the corresponding energy loss by the fragment in traversing this distance is computed. The energy loss is determined from an expression for the stopping power given by Niday (13). By many repetitions of this procedure one can build up an energy deposition or pulse-height spectrum in the ion chamber. A number of foil and substrate thicknesses were calculated in this way before arriving at the final thicknesses.

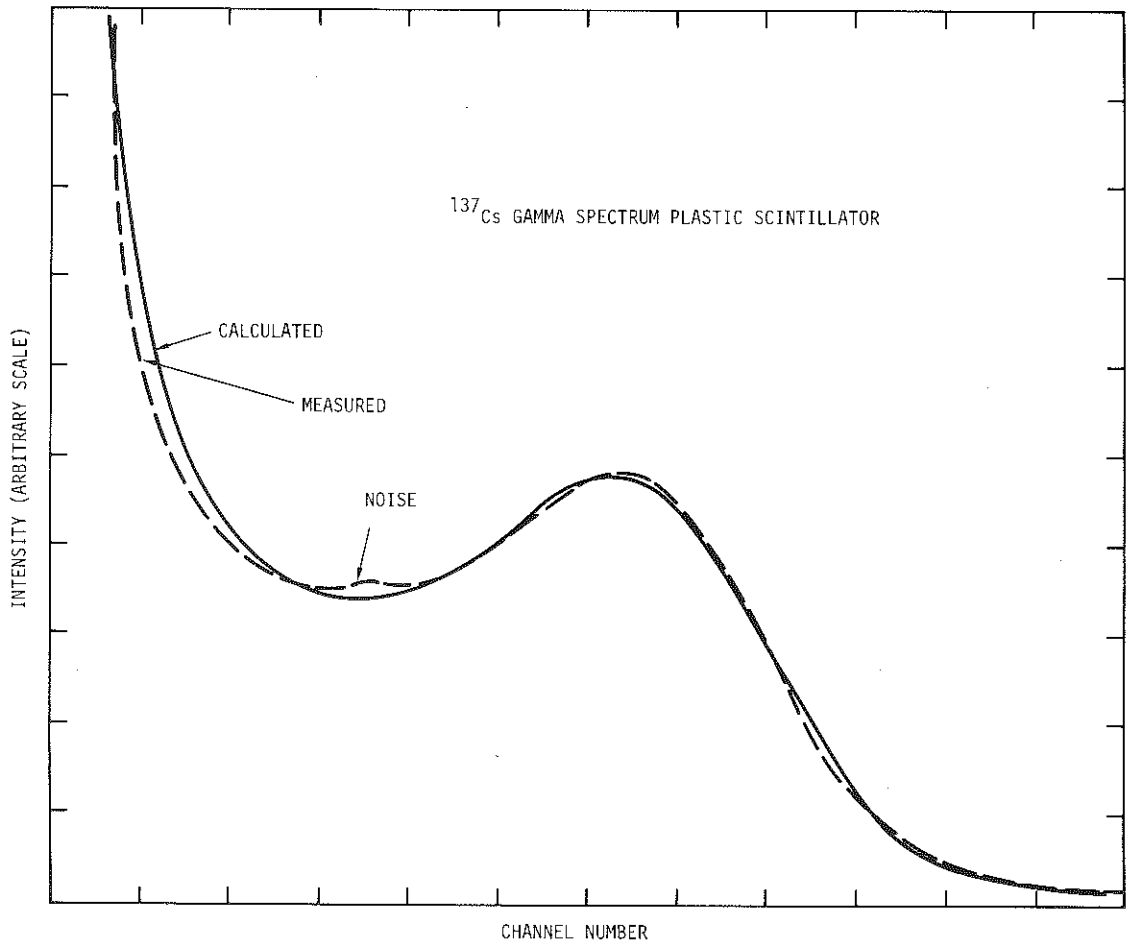


Figure 9. Calculated versus measured $^{137}C_s$ gamma ray spectrum in plastic scintillator

## 3.6 ION CHAMBER RESPONSE

The energy deposition in each component of the scintillator was calculated for the fission product gamma-ray and beta-ray spectra. For the fission product gamma rays, the source spectra were taken from the measurements of Bunney and Sam (5) corresponding to 15 min. and 72 hours after a short irradiation. Although their irradiation time did not correspond to that used for the present experiments, these spectra were the only available at this time. No significant difference was found for the fraction of source energy deposited for these two cases. There was also found to be no difference between the fractional energy depositions of $^{60}Co$ and the fission product gamma rays. The beta rays source spectra used were again the measurements of Tsoulfonidis et al. (6) for their shortest and longest cooling times.

## Section 4

## DATA ANALYSIS

The data acquisition code reports the ratio of the net fission product decay signal to the net $^{60}Co$ standard source signal. The fission product beta and gamma radiation are detected with efficiencies $\varepsilon_\beta$ and $\varepsilon_\gamma$, respectively, and the $^{60}Co$ radiation is detected with efficiency $\varepsilon_C$. Thus, the experimentally measured quantity can be represented as:

$$R = \frac{\varepsilon_\beta E_\beta + \varepsilon_\gamma E_\gamma}{\varepsilon_C E_C} \quad , \tag{1}$$

where E represents the energy emission rate of the respective radiation sources. The efficiency can be calculated with satisfactory accuracy using published differential beta and gamma-ray spectra, but it is necessary to obtain estimates of $E_\beta$ and $E_\gamma$ separately, in order to obtain a correct value of the total decay heat from the measurement.

This is accomplished by inserting an iron liner in the plastic scintillator to absorb the majority of the beta radiation. With the iron in place, we obtain a new measured quantity

$$R_i = \frac{T_{\beta i} E_\beta + \varepsilon_{\gamma i} E_\gamma}{\varepsilon_{C_i} E_C} \quad ,$$

or

$$E_\gamma = \frac{R_i \varepsilon_{C_i} E_C - T_{\beta i} E_\beta}{\varepsilon_{\gamma i}} \quad . \tag{2}$$

The subscript i designates quantities appropriate to the iron liner case. It is important to note here that the values of $\varepsilon_{\gamma i}$ and $\varepsilon_{C_i}$ differ only slightly from the corresponding quantities without the iron, and that the value of the beta transmission is small.

Thus, we can form an estimate of the fission product gamma signal, provided that we can obtain at least a crude estimate of the beta energy. This can be achieved by taking advantage of the fact that the detection efficiency for both radiation sources is high. This allows us to write the total energy emission rate as the measured quantity plus small correction terms, i.e.,

$$S = E_\beta + E_\gamma = R\varepsilon_C E_C + (1-\varepsilon_\beta)E_\beta + (1-\varepsilon_\gamma)E_\gamma \quad . \tag{3}$$

From Eq. 3 we can then form an estimate of the beta energy as

$$E_\beta = S - E_\gamma \quad . \tag{4}$$

Equations 2, 3, and 4 can now be solved by iteration to obtain the beta- and gamma-ray components, as well as the corrected total decay heat.

The magnitudes of the calculated efficiencies used in the iterative solution are indicated in Table 4-1. It is of interest to note that the value of the total fission product decay heat S differs from the measured quantity R by only 1 to 2%. This results from the fact that the fraction of fission product gamma-ray energy escaping from the system is roughly equal to the fraction of the $^{60}Co$ energy that escapes, and that an important contribution to the loss of all three radiation sources is escape from the reentrant hole in the scintillator. This latter effect is geometrical, and hence not dependent on the properties of the spectrum.

Table 4-1

RADIATION DETECTION EFFICIENCIES

| | Without Iron Liner | Cooling Time (sec) | With Iron Liner |
|---|---|---|---|
| $^{60}Co$ | 0.8966 | | 0.8523 |
| Fission | 0.8923 | 900 | 0.8265 |
| Product $\gamma$ | 0.8943 | 259200 | -- |
| Fission | 0.9273 | 0 to 12 | 0.0484 |
| Product $\beta$ | 0.8815 | 10800 to 11100 | 0.0140 |

## Section 5

## RESULTS AND CONCLUSIONS

Before any serious attempt was made to accumulate fission-product decay-heat data, several system checkout experiments were performed. These experiments were used to verify the recording system response time and reproducibility, and to establish activation backgrounds.

The response time measurements involved a special test code (TFH), which reported the time history of the scintillator current before and after the signal control relays were switched, or the programmed power supply was adjusted. In this way, the time for the system to reach equilibrium was established. This time was used as a delay in the acquisition code which followed any operation which made a change in the signal current. In this way, the transient effects due to signal switching and rabbit motion on the measured signal were eliminated.

Another important check was the measurement of the activation background of the rabbit assembly. The rabbits are constructed from materials (polyethylene and mylar) characterized by very low activation cross sections, but the mass of the rabbit is many orders of magnitude greater than that of the sample, and hence even small amounts of activation could be significant. Several measurements were performed, and the net signal obtained was consistently less than 1% of the typical fission product signal. For this reason, no cooling time-dependent background corrections were necessary. The background from natural activity of the $^{235}U$ was also found to be negligible. In some instances, samples were reirradiated after cooling times much longer than the irradiation time. In these cases, a small time-independent background subtraction was made.

As part of the initial system checkout, measurements were made on irradiated aluminum and sodium nitrate samples. The 3.01-MeV beta-ray activity and the 1.80-MeV gamma-ray activity from $^{28}Al$ decays with a 2.24-minute

half-life. The measured signal and the signal corrected for the decay are illustrated in Figure 10. The flat character of the decay-corrected curve indicates that the system is reliably following the decay until very low signal levels are reached. The fission product decay signal is always kept much larger than this minimum value by selecting the proper electrometer sensitivity.

The 1.369- and 2.754-MeV gamma activity from $^{24}Na$ decays with a 15.00 hour half-life. Figure 11 illustrates the decay-corrected data. The low points are those taken with the plastic scintillator only. Again, the flatness of the curve throughout the measured time range tends to confirm the system reliability and freedom from spurious activation.

The linearity of the recording system, as observed at the input to the electrometer, was measured with a precision current source with a nominal linearity of 0.05%. The linearity of the output was better than 0.2% throughout the range used in the measurement.

Since the scintillator was constructed for use with a linear accelerator, the last five dynodes of all the photomultipliers are supplied in parallel from a low impedance power supply. This feature eliminates overloading effects for signals orders of magnitude larger than those encountered in this work. As a confirmation of this, two gamma sources, with activities in the millicurie range, were measured separately and together to confirm that the sum signal equaled the sum of the individual signals.

The fission product, decay-heat data for a 24-hour irradiation time is listed in Tables 5-1, 5-2, 5-3, and illustrated in Figures 12 and 13. The data in Figure 14 have been divided by a calculation based on infinite irradiation fission product summation calculations by Spinrad (14). The comparison involves the differentiation of the decay-heat curve which tends to magnify small errors in the calculation for long cooling times. For this reason, the discrepancies from a flat curve observed at long times are probably due to this effect. A much better standard of comparison would be a calculation based on the 24-hour irradiation used here. The discrepancy for times less than 20 seconds is significant and represents the inadequacy of the short cooling time differential data used in the calculations.

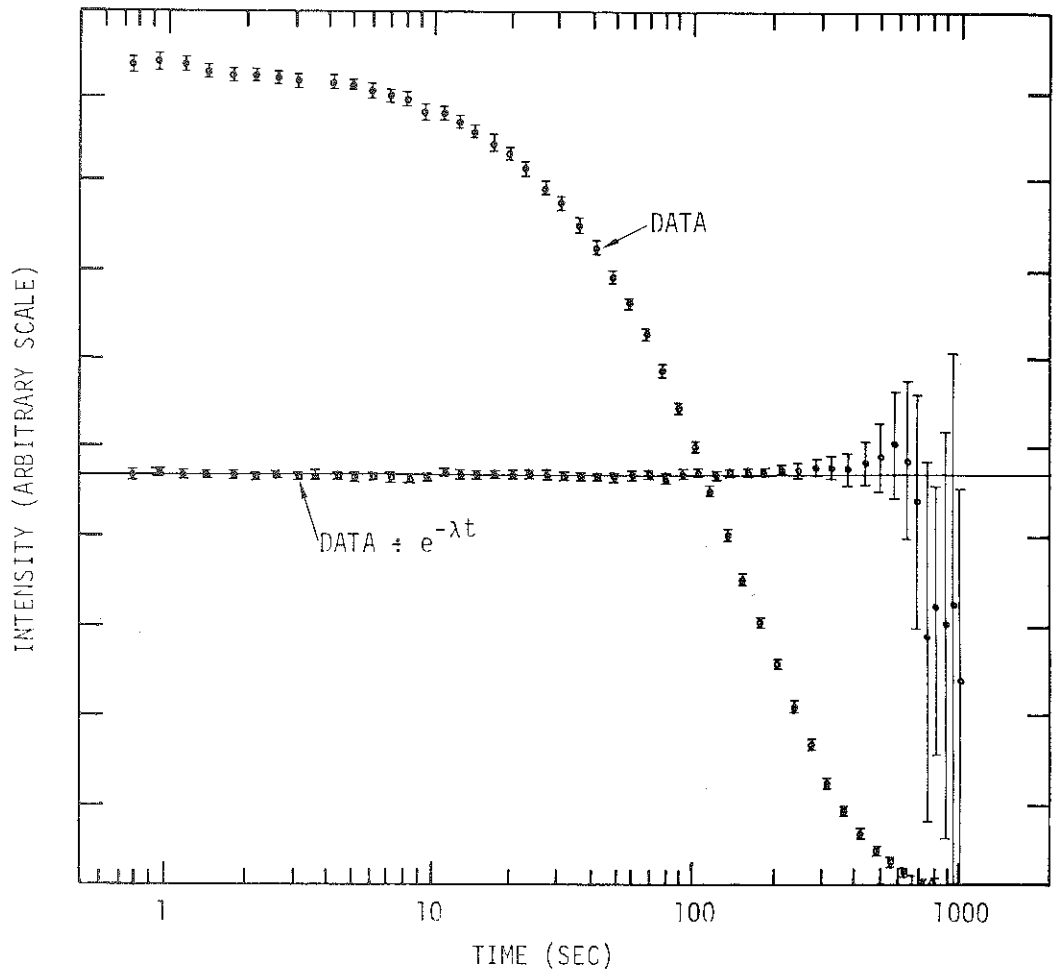


Figure 10. $^{28}$Aℓ decay data, and data corrected for 2.24 min. half life.

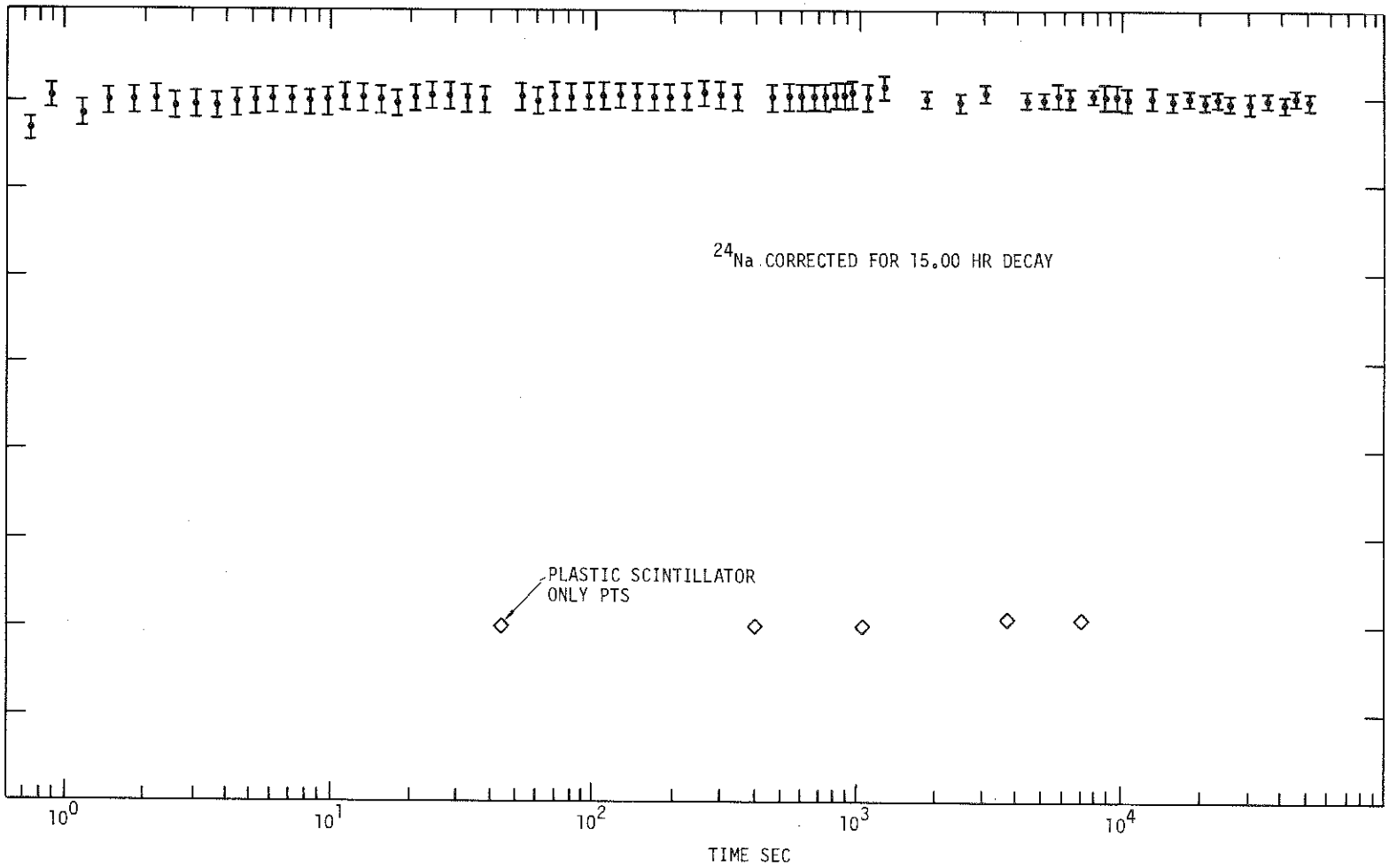


Figure 11. $^{24}$Na data corrected for 15.00 hr half life.

Table 5-1. Total Decay Heat for 24 Hr. Irradiation

| TIME | $\frac{P}{P_0}$ | STD DEV | MEV/FIS | STD DEV |
|---|---|---|---|---|
| .75 | .0553811 | .0011422 | 11.0762234 | .2284393 |
| 1.00 | .0549857 | .0011341 | 10.9971466 | .2268104 |
| 1.25 | .0541670 | .0011172 | 10.8334103 | .2234378 |
| 1.65 | .0530926 | .0010951 | 10.6185226 | .2190117 |
| 2.00 | .0518667 | .0010698 | 10.3733501 | .2139617 |
| 2.45 | .0512200 | .0010565 | 10.2440033 | .2112974 |
| 2.95 | .0497130 | .0010254 | 9.9426003 | .2050892 |
| 3.60 | .0484745 | .0009999 | 9.6948986 | .1999873 |
| 4.25 | .0473659 | .0009771 | 9.4731789 | .1954204 |
| 5.00 | .0462394 | .0009539 | 9.2478886 | .1907800 |
| 5.95 | .0450486 | .0009294 | 9.0097141 | .1858743 |
| 7.00 | .0438629 | .0009049 | 8.7725754 | .1809900 |
| 8.25 | .0427681 | .0008824 | 8.5536270 | .1764803 |
| 9.65 | .0415503 | .0008573 | 8.3100605 | .1714635 |
| 11.25 | .0402680 | .0008309 | 8.0535984 | .1661812 |
| 13.10 | .0393368 | .0008117 | 7.8673677 | .1623454 |
| 15.25 | .0381773 | .0007878 | 7.6354628 | .1575690 |
| 17.80 | .0370049 | .0007637 | 7.4009790 | .1527394 |
| 20.65 | .0359409 | .0007418 | 7.1881828 | .1483566 |
| 24.10 | .0348611 | .0007195 | 6.9722281 | .1439087 |
| 27.95 | .0338116 | .0006979 | 6.7623110 | .1395852 |
| 32.50 | .0328099 | .0006773 | 6.5619831 | .1354593 |
| 37.70 | .0318368 | .0006573 | 6.3673677 | .1314510 |
| 43.75 | .0307457 | .0006348 | 6.1491385 | .1269565 |
| 60.85 | .0284549 | .0005876 | 5.6909819 | .1175205 |
| 70.25 | .0275579 | .0005691 | 5.5115728 | .1138257 |
| 81.10 | .0265921 | .0005492 | 5.3184109 | .1098476 |
| 93.70 | .0256855 | .0005306 | 5.1370935 | .1061134 |
| 108.30 | .0247979 | .0005123 | 4.9595881 | .1024578 |
| 125.15 | .0239035 | .0004939 | 4.7807007 | .0987739 |
| 144.70 | .0229985 | .0004752 | 4.5996952 | .0950464 |
| 167.35 | .0221702 | .0004582 | 4.4340448 | .0916352 |
| 193.55 | .0213661 | .0004416 | 4.2732143 | .0883233 |
| 223.90 | .0206092 | .0004260 | 4.1218319 | .0852060 |
| 259.20 | .0198255 | .0004099 | 3.9650903 | .0819785 |
| 300.25 | .0191092 | .0003951 | 3.8218322 | .0790287 |
| 347.90 | .0184030 | .0003806 | 3.6805911 | .0761205 |
| 403.15 | .0177102 | .0003663 | 3.5420480 | .0732680 |
| 542.70 | .0163345 | .0003380 | 3.2669001 | .0676032 |
| 621.50 | .0156395 | .0003237 | 3.1279087 | .0647418 |
| 700.30 | .0150673 | .0003119 | 3.0134516 | .0623856 |
| 779.10 | .0145749 | .0003018 | 2.9149761 | .0603585 |
| 857.95 | .0141286 | .0002926 | 2.8257184 | .0585212 |
| 936.75 | .0137065 | .0002839 | 2.7413044 | .0567838 |
| 1015.55 | .0132765 | .0002751 | 2.6553020 | .0550137 |
| 1094.30 | .0129297 | .0002679 | 2.5859361 | .0535861 |
| 1253.75 | .0123057 | .0002551 | 2.4611330 | .0510178 |
| 1604.15 | .0110864 | .0001732 | 2.2172804 | .0346372 |
| 1845.95 | .0104095 | .0001553 | 2.0819039 | .0310653 |
| 2169.15 | .0096874 | .0001291 | 1.9374800 | .0258239 |
| 2395.75 | .0094175 | .0000720 | 1.8835027 | .0143917 |
| 2721.30 | .0086889 | .0001460 | 1.7377775 | .0291977 |
| 2952.90 | .0084180 | .0001876 | 1.6836028 | .0375126 |
| 3494.55 | .0078769 | .0001149 | 1.5753818 | .0229704 |
| 3808.25 | .0075193 | .0000441 | 1.5038512 | .0088285 |
| 4033.65 | .0073480 | .0000742 | 1.4695919 | .0148339 |
| 4353.65 | .0070220 | .0000803 | 1.4043965 | .0160510 |
| 4585.45 | .0068009 | .0001069 | 1.3601878 | .0213751 |
| 4898.10 | .0065673 | .0000624 | 1.3134530 | .0124821 |
| 5128.30 | .0064735 | .0000767 | 1.2946970 | .0153405 |
| 5570.25 | .0061629 | .0001158 | 1.2325764 | .0231693 |
| 6057.25 | .0058888 | .0001021 | 1.1777532 | .0204179 |
| 7033.45 | .0054012 | .0000883 | 1.0802500 | .0176600 |
| 7547.80 | .0051910 | .0001175 | 1.0382090 | .0235095 |
| 8054.20 | .0048531 | .0004842 | .9706173 | .0968361 |
| 8562.00 | .0048393 | .0000840 | .9678662 | .0168097 |
| 9390.05 | .0045287 | .0000697 | .9057499 | .0139427 |
| 10414.40 | .0043358 | .0000747 | .8671652 | .0149333 |
| 12906.90 | .0038247 | .0000760 | .7649305 | .0151937 |
| 15410.25 | .0033259 | .0001562 | .6651802 | .0312367 |
| 17891.80 | .0030325 | .0000907 | .6064954 | .0181363 |
| 20390.50 | .0027993 | .0000480 | .5598506 | .0095978 |
| 22914.50 | .0025887 | .0000615 | .5177469 | .0123053 |
| 25406.50 | .0023607 | .0000603 | .4721451 | .0120598 |
| 30409.95 | .0020258 | .0000564 | .4051564 | .0112825 |
| 35411.60 | .0018389 | .0000612 | .3677787 | .0122368 |
| 40408.70 | .0016244 | .0000509 | .3248795 | .0101867 |
| 45416.80 | .0014543 | .0000482 | .2908691 | .0096318 |
| 50413.55 | .0013309 | .0000498 | .2661722 | .0099672 |
| 60398.85 | .0010954 | .0000404 | .2190869 | .0080850 |
| 70421.05 | .0009897 | .0000464 | .1979430 | .0092711 |
| 89320.22 | .0007294 | .0000108 | .1458707 | .0021546 |
| 97189.97 | .0006716 | .0000521 | .1343202 | .0104102 |
| 100383.75 | .0006374 | .0000316 | .1274749 | .0063259 |
| 102018.66 | .0006206 | .0000173 | .1241135 | .0034661 |
| 151276.25 | .0003773 | .0000178 | .0754611 | .0035632 |

Table 5-2 Gamma-Ray component of Decay Heat for 24 Hr Irradiation.

| TIME | $\frac{P}{P_0}$ | STD DEV | MEV/FIS | STD DEV |
|---|---|---|---|---|
| .75 | .0277426 | .0007014 | 5.5485153 | .1402885 |
| 1.00 | .0270255 | .0006752 | 5.4051046 | .1350497 |
| 1.25 | .0266771 | .0006754 | 5.3354187 | .1350805 |
| 1.65 | .0263352 | .0006528 | 5.2670317 | .1305657 |
| 2.00 | .0258190 | .0006531 | 5.1637993 | .1306175 |
| 2.45 | .0251658 | .0003614 | 5.0331516 | .0722824 |
| 2.95 | .0245987 | .0003606 | 4.9197321 | .0721143 |
| 3.60 | .0243091 | .0003571 | 4.8618174 | .0714284 |
| 4.25 | .0237884 | .0003486 | 4.7576761 | .0697198 |
| 5.00 | .0232604 | .0003435 | 4.6520796 | .0686971 |
| 5.95 | .0225706 | .0003320 | 4.5141268 | .0663961 |
| 7.00 | .0222941 | .0003304 | 4.4588232 | .0660889 |
| 8.25 | .0217335 | .0003172 | 4.3467093 | .0634389 |
| 9.65 | .0212136 | .0003154 | 4.2427282 | .0630789 |
| 11.25 | .0206998 | .0003073 | 4.1399508 | .0614506 |
| 13.10 | .0203372 | .0003045 | 4.0674314 | .0608971 |
| 15.25 | .0197989 | .0002924 | 3.9597778 | .0584800 |
| 17.80 | .0193305 | .0002874 | 3.8660965 | .0574759 |
| 20.65 | .0188593 | .0002803 | 3.7718644 | .0560666 |
| 24.10 | .0182970 | .0002744 | 3.6593966 | .0548715 |
| 27.95 | .0177974 | .0002677 | 3.5594711 | .0535450 |
| 32.50 | .0172619 | .0002612 | 3.4523845 | .0522482 |
| 37.70 | .0167335 | .0002545 | 3.3467026 | .0508924 |
| 43.75 | .0162234 | .0002482 | 3.2446780 | .0496330 |
| 60.85 | .0150215 | .0002326 | 3.0043073 | .0465131 |
| 70.25 | .0146078 | .0002276 | 2.9215641 | .0455234 |
| 81.10 | .0141056 | .0002207 | 2.8211150 | .0441499 |
| 93.70 | .0136059 | .0002143 | 2.7211785 | .0428634 |
| 108.30 | .0131117 | .0002079 | 2.6223421 | .0415764 |
| 125.15 | .0126657 | .0002021 | 2.5331311 | .0404196 |
| 144.70 | .0122292 | .0001964 | 2.4458356 | .0392780 |
| 167.35 | .0117604 | .0001902 | 2.3520799 | .0380306 |
| 193.55 | .0113129 | .0001843 | 2.2625895 | .0368538 |
| 223.90 | .0109375 | .0001794 | 2.1875048 | .0358762 |
| 259.20 | .0105113 | .0001737 | 2.1022534 | .0347391 |
| 300.25 | .0101147 | .0001685 | 2.0229335 | .0336978 |
| 347.90 | .0097327 | .0001635 | 1.9465468 | .0326909 |
| 403.15 | .0093795 | .0001588 | 1.8758912 | .0317604 |
| 542.70 | .0086538 | .0001492 | 1.7307599 | .0298303 |
| 621.50 | .0083292 | .0001449 | 1.6658337 | .0289704 |
| 700.30 | .0080504 | .0001377 | 1.6100855 | .0275370 |
| 779.10 | .0077925 | .0001343 | 1.5585077 | .0268534 |
| 857.95 | .0075349 | .0001321 | 1.5069814 | .0264104 |
| 936.75 | .0073754 | .0001292 | 1.4750865 | .0258350 |
| 1015.55 | .0071533 | .0001268 | 1.4306533 | .0253617 |
| 1094.30 | .0069765 | .0001227 | 1.3952940 | .0245487 |
| 1253.75 | .0066755 | .0000880 | 1.3351090 | .0175977 |
| 1604.15 | .0059342 | .0000880 | 1.1868482 | .0175967 |
| 1845.95 | .0055670 | .0000313 | 1.1134019 | .0062538 |
| 2169.15 | .0052938 | .0001151 | 1.0587535 | .0230222 |
| 2395.75 | .0050341 | .0001150 | 1.0068259 | .0229957 |
| 2721.30 | .0047482 | .0000643 | .9496464 | .0128623 |
| 2952.90 | .0045457 | .0000737 | .9091328 | .0147323 |
| 3494.55 | .0041304 | .0000874 | .8260840 | .0174840 |
| 3808.25 | .0039410 | .0000875 | .7881993 | .0175033 |
| 4033.65 | .0038168 | .0000875 | .7633679 | .0175056 |
| 4353.65 | .0036569 | .0000769 | .7313844 | .0153736 |
| 4585.45 | .0035469 | .0000769 | .7093819 | .0153884 |
| 4898.10 | .0034087 | .0000495 | .6817484 | .0099080 |
| 5128.30 | .0033132 | .0000495 | .6626335 | .0099068 |
| 5570.25 | .0031718 | .0000709 | .6343582 | .0141734 |
| 6057.25 | .0030149 | .0000665 | .6029879 | .0132980 |
| 7033.45 | .0027629 | .0000865 | .5525895 | .0173050 |
| 7547.80 | .0026567 | .0000867 | .5313323 | .0173400 |
| 8054.20 | .0025649 | .0000724 | .5129893 | .0144838 |
| 8562.00 | .0024651 | .0000724 | .4930256 | .0144874 |
| 9390.05 | .0023279 | .0000717 | .4655878 | .0143309 |
| 10414.40 | .0021240 | .0000538 | .4248092 | .0107570 |
| 12906.90 | .0018111 | .0000284 | .3622164 | .0056861 |
| 15410.25 | .0015979 | .0000384 | .3195757 | .0076893 |
| 17891.80 | .0014119 | .0000370 | .2823859 | .0073920 |
| 20390.50 | .0012781 | .0000463 | .2556276 | .0092641 |
| 22914.50 | .0011718 | .0000181 | .2343553 | .0036143 |
| 25406.50 | .0010839 | .0000309 | .2167756 | .0061824 |
| 30409.95 | .0009536 | .0000283 | .1907295 | .0056670 |
| 35411.60 | .0008374 | .0000288 | .1674798 | .0057507 |
| 40408.70 | .0007711 | .0000278 | .1542211 | .0055615 |
| 45416.80 | .0006967 | .0000156 | .1393450 | .0031261 |
| 50413.55 | .0006346 | .0000229 | .1269120 | .0045879 |
| 60398.85 | .0005481 | .0000251 | .1096294 | .0050159 |
| 70421.05 | .0004621 | .0000270 | .0924281 | .0053913 |
| 89320.22 | .0003711 | .0000197 | .0742192 | .0039407 |
| 97189.97 | .0003450 | .0000218 | .0689936 | .0043685 |
| 100383.75 | .0003359 | .0000219 | .0671818 | .0043721 |
| 102018.66 | .0003309 | .0000185 | .0661836 | .0037001 |
| 151276.25 | .0002145 | .0000272 | .0429044 | .0054493 |

Table 5-3. Beta Component of Decay Heat for 24 Hr Irradiation.

| TIME | $\frac{P}{P_O}$ | STD DEV | MEV/FIS | STD DEV |
|---|---|---|---|---|
| .75 | .0276385 | .0013404 | 5.5277090 | .2680773 |
| 1.00 | .0279602 | .0013199 | 5.5920410 | .2639723 |
| 1.25 | .0274900 | .0013055 | 5.4979906 | .2610961 |
| 1.65 | .0267575 | .0012749 | 5.3514910 | .2549775 |
| 2.00 | .0260478 | .0012534 | 5.2095499 | .2506801 |
| 2.45 | .0260543 | .0011166 | 5.2108507 | .2233189 |
| 2.95 | .0251143 | .0010870 | 5.0228682 | .2173984 |
| 3.60 | .0241654 | .0010618 | 4.8330803 | .2123604 |
| 4.25 | .0235775 | .0010374 | 4.7155027 | .2074849 |
| 5.00 | .0229790 | .0010139 | 4.5958090 | .2027716 |
| 5.95 | .0224779 | .0009869 | 4.4955883 | .1973771 |
| 7.00 | .0215688 | .0009634 | 4.3137531 | .1926788 |
| 8.25 | .0210346 | .0009377 | 4.2069178 | .1875361 |
| 9.65 | .0203367 | .0009135 | 4.0673313 | .1826983 |
| 11.25 | .0195682 | .0008859 | 3.9136486 | .1771789 |
| 13.10 | .0189997 | .0008670 | 3.7999363 | .1733912 |
| 15.25 | .0183784 | .0008404 | 3.6756845 | .1680711 |
| 17.80 | .0176744 | .0008160 | 3.5348825 | .1631956 |
| 20.65 | .0170816 | .0007930 | 3.4163184 | .1585974 |
| 24.10 | .0165642 | .0007701 | 3.3128314 | .1540149 |
| 27.95 | .0160142 | .0007475 | 3.2028399 | .1495029 |
| 32.50 | .0155480 | .0007259 | 3.1095982 | .1451864 |
| 37.70 | .0151033 | .0007048 | 3.0206652 | .1409588 |
| 43.75 | .0145223 | .0006816 | 2.9044604 | .1363135 |
| 60.85 | .0134334 | .0006320 | 2.6866751 | .1263904 |
| 70.25 | .0129500 | .0006130 | 2.5900087 | .1225915 |
| 81.10 | .0124865 | .0005919 | 2.4972959 | .1183879 |
| 93.70 | .0120796 | .0005722 | 2.4159150 | .1144435 |
| 108.30 | .0116862 | .0005529 | 2.3372455 | .1105722 |
| 125.15 | .0112378 | .0005336 | 2.2475696 | .1067241 |
| 144.70 | .0107693 | .0005142 | 2.1538601 | .1028425 |
| 167.35 | .0104098 | .0004961 | 2.0819650 | .0992136 |
| 193.55 | .0100531 | .0004785 | 2.0106249 | .0957038 |
| 223.90 | .0096716 | .0004623 | 1.9343269 | .0924509 |
| 259.20 | .0093142 | .0004452 | 1.8628366 | .0890352 |
| 300.25 | .0089945 | .0004296 | 1.7988985 | .0859132 |
| 347.90 | .0086702 | .0004142 | 1.7340443 | .0828434 |
| 403.15 | .0083308 | .0003993 | 1.6661565 | .0798556 |
| 542.70 | .0076807 | .0003695 | 1.5361402 | .0738920 |
| 621.50 | .0073104 | .0003546 | 1.4620752 | .0709280 |
| 700.30 | .0070168 | .0003410 | 1.4033661 | .0681927 |
| 779.10 | .0067823 | .0003303 | 1.3564687 | .0660625 |
| 857.95 | .0065937 | .0003210 | 1.3187370 | .0642047 |
| 936.75 | .0063311 | .0003119 | 1.2662179 | .0623847 |
| 1015.55 | .0061232 | .0003029 | 1.2246485 | .0605783 |
| 1094.30 | .0059532 | .0002947 | 1.1906421 | .0589415 |
| 1253.75 | .0056301 | .0002698 | 1.1260242 | .0539675 |
| 1604.15 | .0051522 | .0001943 | 1.0304325 | .0388508 |
| 1845.95 | .0048425 | .0001584 | .9685019 | .0316885 |
| 2169.15 | .0043936 | .0001730 | .8787265 | .0345961 |
| 2395.75 | .0043834 | .0001356 | .8766768 | .0271279 |
| 2721.30 | .0039407 | .0001595 | .7881311 | .0319053 |
| 2952.90 | .0038723 | .0002015 | .7744700 | .0403018 |
| 3494.55 | .0037465 | .0001443 | .7492976 | .0288674 |
| 3808.25 | .0035783 | .0000980 | .7156519 | .0196038 |
| 4033.65 | .0035311 | .0001147 | .7062240 | .0229454 |
| 4353.65 | .0033651 | .0001111 | .6730120 | .0222257 |
| 4585.45 | .0032540 | .0001317 | .6508060 | .0263381 |
| 4898.10 | .0031585 | .0000797 | .6317047 | .0159364 |
| 5128.30 | .0031603 | .0000913 | .6320636 | .0182613 |
| 5570.25 | .0029911 | .0001358 | .5982182 | .0271606 |
| 6057.25 | .0028738 | .0001218 | .5747654 | .0243665 |
| 7033.45 | .0026383 | .0001236 | .5276605 | .0247253 |
| 7547.80 | .0025344 | .0001461 | .5068767 | .0292125 |
| 8054.20 | .0022881 | .0004896 | .4576281 | .0979133 |
| 8562.00 | .0023742 | .0001110 | .4748406 | .0221913 |
| 9390.05 | .0022008 | .0001000 | .4401621 | .0199943 |
| 10414.40 | .0022118 | .0000920 | .4423561 | .0184042 |
| 12906.90 | .0020136 | .0000811 | .4027140 | .0162229 |
| 15410.25 | .0017280 | .0001608 | .3456045 | .0321692 |
| 17891.80 | .0016205 | .0000979 | .3241094 | .0195849 |
| 20390.50 | .0015211 | .0000667 | .3042229 | .0133395 |
| 22914.50 | .0014170 | .0000641 | .2833917 | .0128251 |
| 25406.50 | .0012768 | .0000678 | .2553694 | .0135521 |
| 30409.95 | .0010721 | .0000631 | .2144269 | .0126258 |
| 35411.60 | .0010015 | .0000676 | .2002989 | .0135207 |
| 40408.70 | .0008533 | .0000580 | .1706583 | .0116060 |
| 45416.80 | .0007576 | .0000506 | .1515241 | .0101264 |
| 50413.55 | .0006963 | .0000549 | .1392602 | .0109724 |
| 60398.85 | .0005473 | .0000476 | .1094575 | .0095146 |
| 70421.05 | .0005276 | .0000536 | .1055149 | .0107247 |
| 89320.22 | .0003583 | .0000225 | .0716516 | .0044913 |
| 97189.97 | .0003266 | .0000564 | .0653266 | .0112896 |
| 100383.75 | .0003015 | .0000384 | .0602931 | .0076898 |
| 102018.66 | .0002896 | .0000254 | .0579299 | .0050700 |
| 151276.25 | .0001628 | .0000326 | .0325567 | .0065108 |

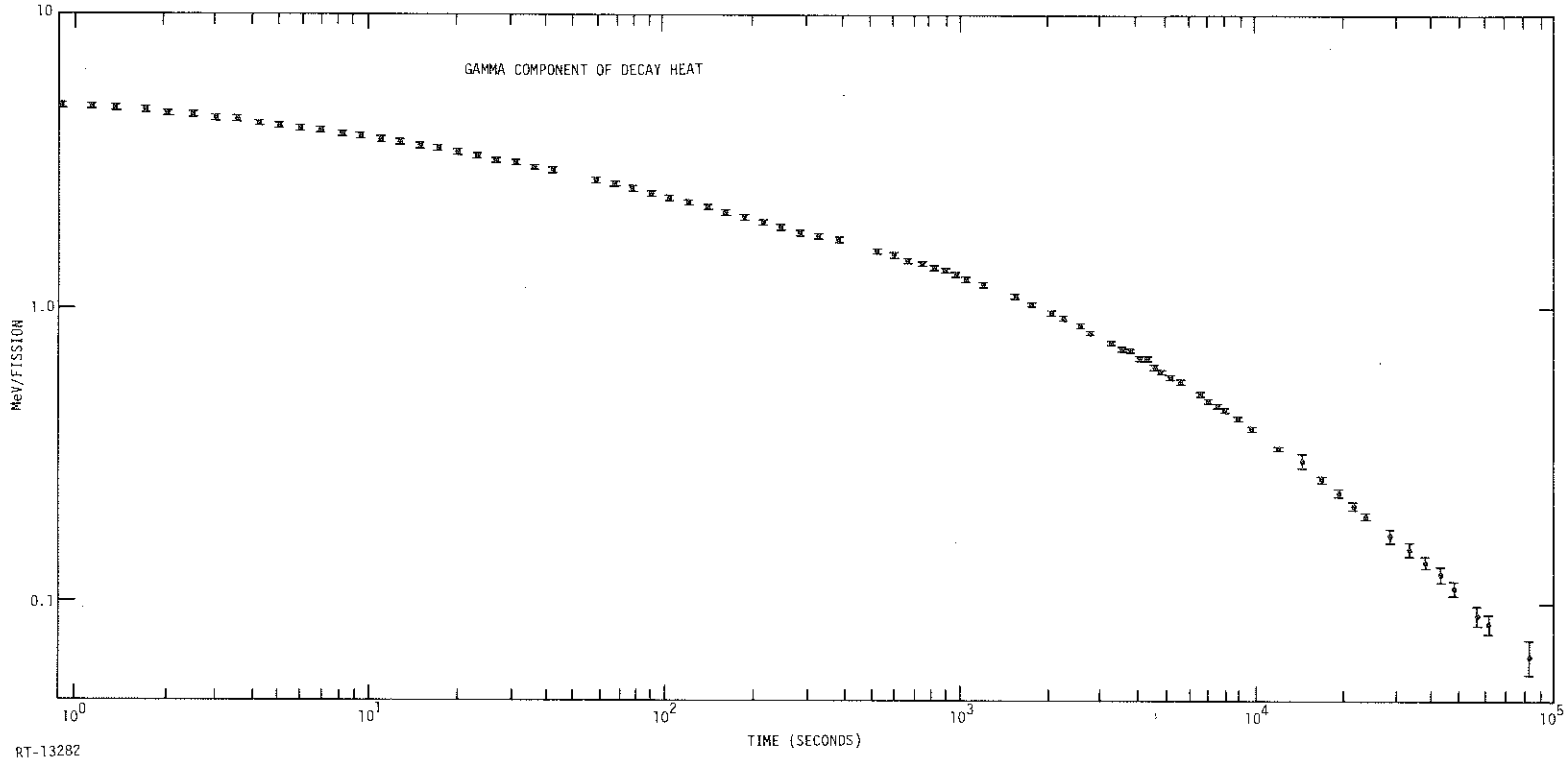


Figure 12. Gamma-ray component of decay heat for 24 hour irradiation.

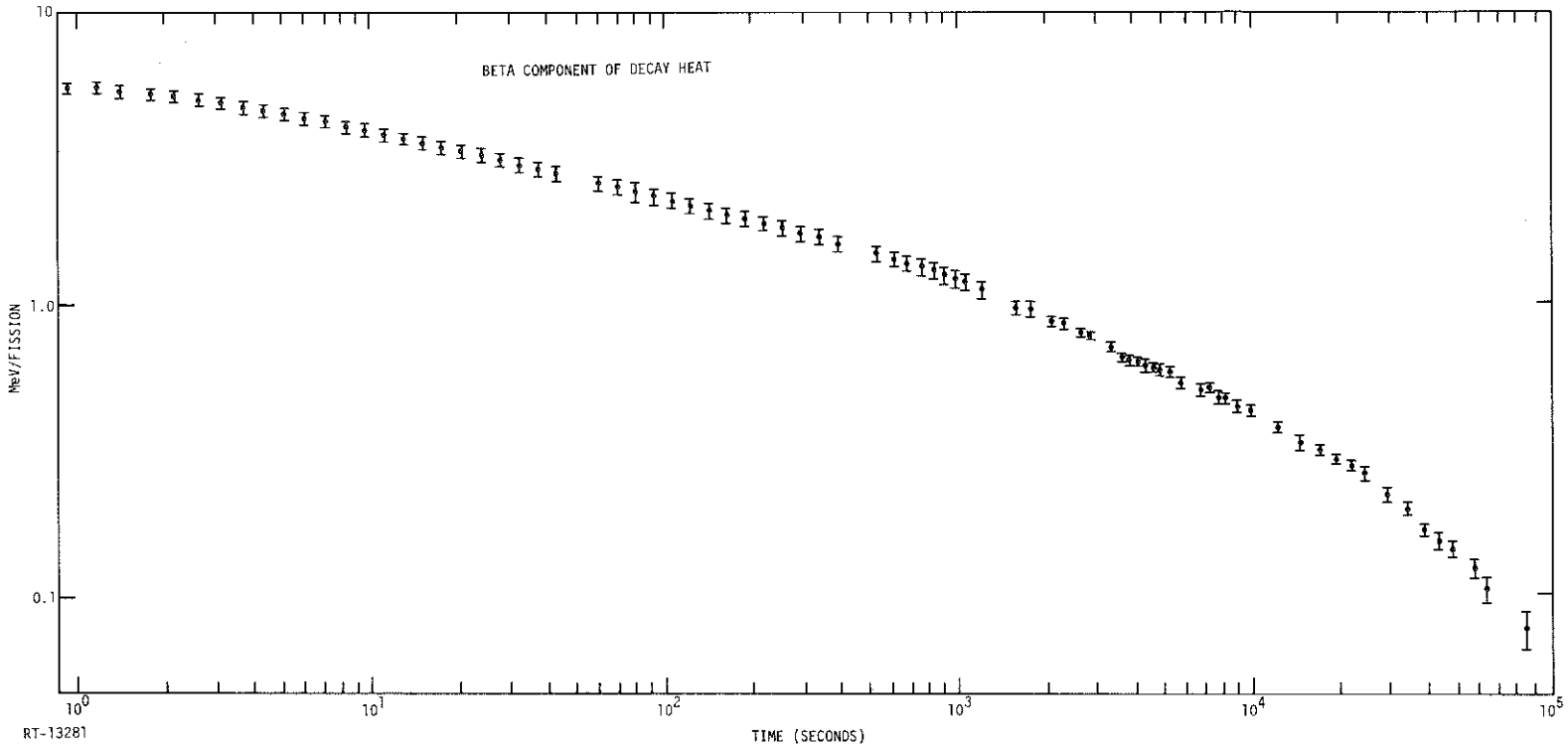


Figure 13. Beta-ray component of decay heat for 24 hour irradiation.

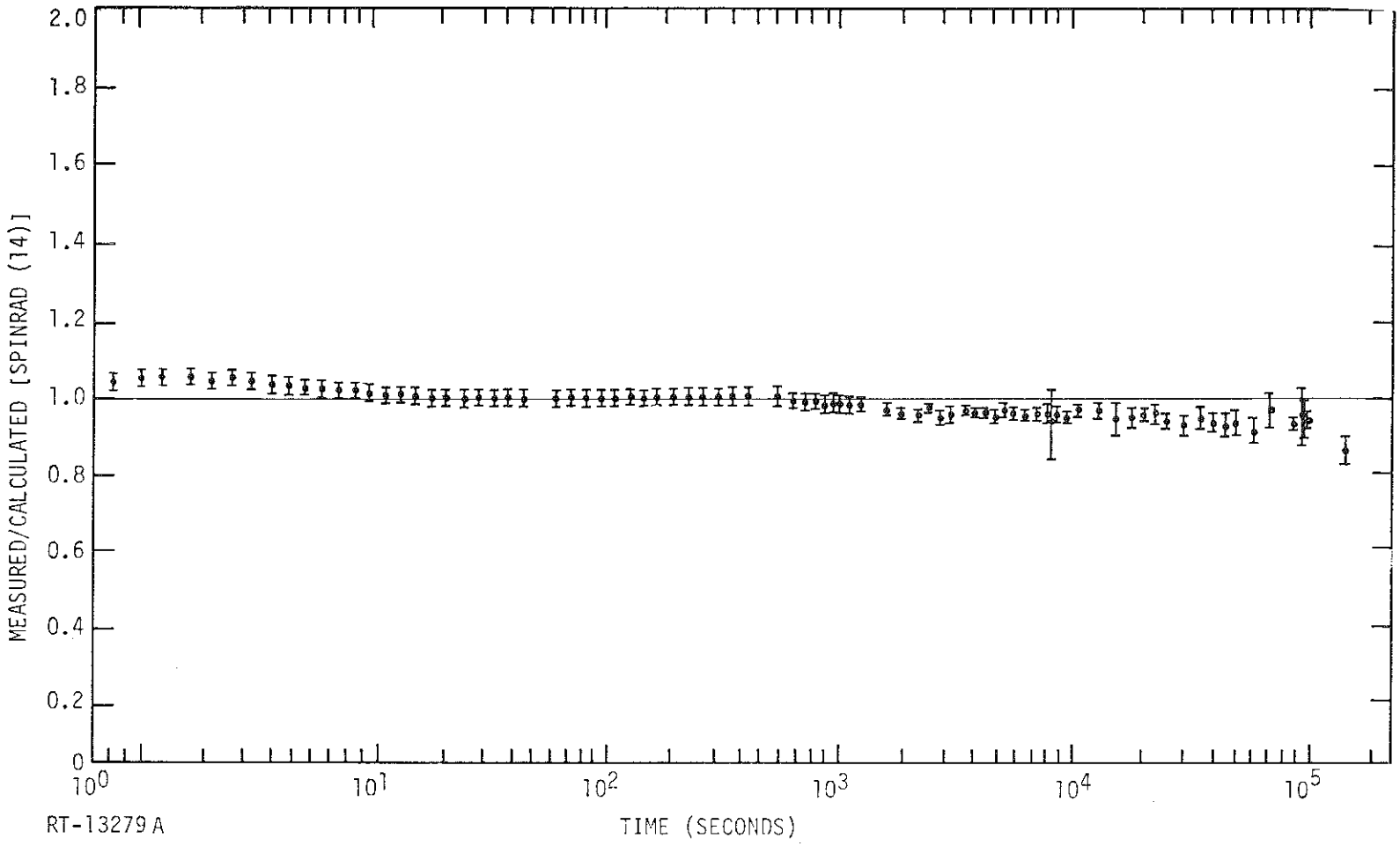


Figure 14. Twenty-four-hour fission product decay heat data divided by calculated value (Ref. 14).

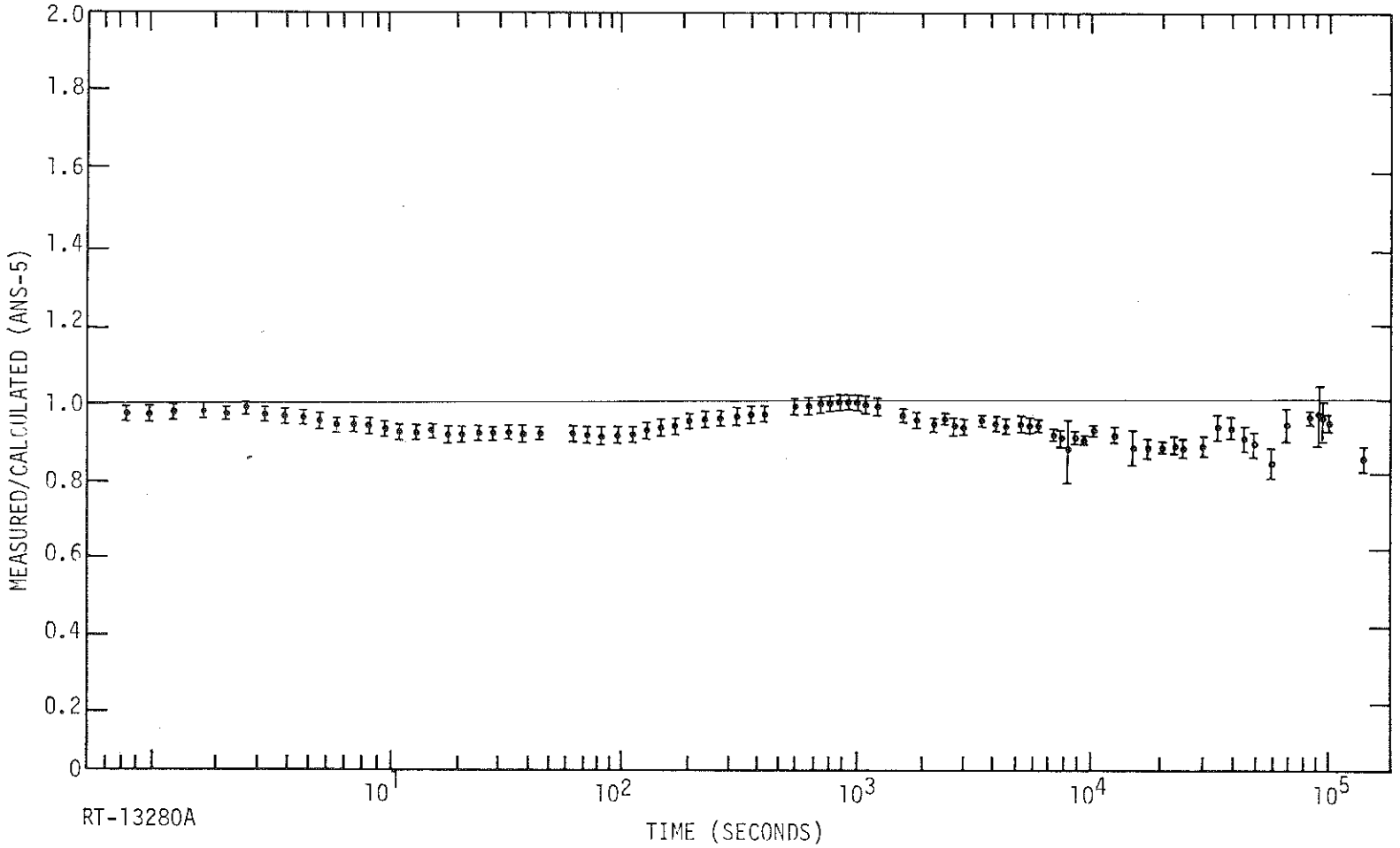


Figure 15. Twenty-four-hour fission product decay heat data divided by ANS-5 standard.

Figure 15 shows the comparison of the data divided by the ANS-5 standard (15).

The systematic uncertainties in the normalization are illustrated in Table 5-4. The indicated net systematic uncertainty of 2.4% is intended to represent one standard deviation. This systematic uncertainty was not included in the standard deviations listed in Tables 5-1, 5-2 and 5-3.

The present data represent a significant improvement in the quality of fission-product, decay-heat values. However, the present results do not represent the best possible accuracy which might be achieved with the present techniques. In particular, further studies of the plastic scintillator response and the effect of scintillator imbalance are in order. In addition, the availability of an adequate supply of ion chamber foils would eliminate the cross normalization uncertainty. A chemical separation of an ion chamber irradiated foil would provide a useful intercomparison of fission rate determinations. In addition, intercomparison of standard $^{60}Co$ sources made at laboratories other than NBS would serve to lend confidence in the standard source used in these measurements.

The possibility of fission product escape from the encapsulated samples requires further investigation. The large contribution of the noble gases to the gamma-ray signal at times $>10^3$ seconds imposes severe requirements on the methods used for encapsulation. Still another improvement that can be made is a more accurate time dependent correction for beta ray energy loss in the samples. For this purpose improved beta spectra corresponding to the 24 hour irradiation would be necessary.

It is anticipated that these and other improvements will be made to the $^{235}U$ results during the course of the $^{239}Pu$ decay heat program now in progress.

ACKNOWLEDGEMENTS

We wish to thank Mr. W.E. Gober for his able assistance in apparatus fabrication and in the performance of these measurements. We would also like to thank Prof. B. Spinrad and his students at Oregon State University for providing calculated decay heat values.

Table 5-4.

EXPERIMENTAL NORMALIZATION UNCERTAINTIES IN NUCLEAR CALORIMETER RESULTS

| | Correction (%) | Net Uncertainty (%) |
|---|---|---|
| SCINTILLATOR MEASUREMENTS | | |
| Beta Absorption in Sample | 6.0 | 0.6 |
| Gamma Energy Escape (Relative) | 0.2 | 0.5 |
| Uniformity of Scintillator Response | - | 0.5 |
| Normalization to Ion Chamber | - | 1.2 |
| $^{60}Co$ Standard Source Activity | - | 1.4 |
| ION CHAMBER NORMALIZATION | | |
| Bias Efficiency | 4.0 | 1.0 |
| Dead Time | 19.7 | 0.4 |
| Fission Product Escape | - | 0.5 |
| Fission Rate Reproducibility | - | 0.2 |
| | NET = | 2.4 |

REFERENCES


1. A. M. Perry, F. C. Maienschein, and D. R. Vondy, ORNL-TM-4197, Oak Ridge National Laboratory (October 1973).

2. B. I. Spinrad, "Evaluation of Fission Product After-Heat," Annual Report NUREG-75/099 (November 1975).

3. S. B. Gunst, D. E. Conway, and J. C. Conner, Nucl. Sci. Eng. 56, 241 (1975).

4. M. Lott, et al., Bulletin D'Information Scientifiques et Techniques 181, 51 (1973).

5. L. R. Bunney and D. Sam, Nucl. Sci. Eng. 39, 81 (1970).

6. N. Tsoulfanidis, B. W. Wehring, and M. E. Wyman, Nucl. Sci. Eng. 43, 42 (1971).

7. E. Haddad, R. B. Walton, S. J. Friesenhahn, and W. M. Lopez, Nucl. Instr. and Meth. 31, 125 (1964).

8. S. J. Friesenhahn, Rev. Sci. Instr. 42, 1016 (1971).

9. H. M. Colbert, "SANDYL: A Computer Program for Calculating Combined Photon-Electron Transport in Complex Systems," Sandia Report SLL-74-0012 (1974).

10. M. J. Berger, in Methods of Computational Physics, eds. B. Alder, S. Fernbach, and M. Rotenberg (Academic Press, New York, 1963), Vol. 1, p. 135.

11. S. T. Hsue, Thesis, Indiana University, 1967 (unpublished).

12. H. W. Schmitt, J. H. Neiler, and F. J. Walter, Phys. Rev. 141, 1146 (1966).

13. J. B. Niday, Phys. Rev. 121, 1471 (1961).

14. B. I. Spinrad, private communication.

15. "Decay Energy Release Rates Following Shutdown of Uranium-Fueled Thermal Reactors", Proposed ANS Standard, Approved by Subcommittee ANS-5, October, 1971, Revised October, 1973.

EPRI NP-180

February 1976



# $^{235}U$ Fission Product Decay Heat from 1 to $10^5$ Seconds